Available online at www.sciencedirect.com

ScienceDirect

Advances in Space Research 65 (2020) 2435–2455

ADVANCES IN SPACE RESEARCH (a COSPAR publication)

www.elsevier.com/locate/asr

Fuzzy energy-based dual contours model for automated coronal hole detection in SDO/AIA solar disk images

Sanmoy Bandyopadhyay, Saurabh Das *, Abhirup Datta

Discipline of Astronomy, Astrophysics and Space Engineering, Indian Institute of Technology, Indore, Simrol, Indore 453552, India

Received 19 October 2019; received in revised form 9 January 2020; accepted 11 February 2020
Available online 19 February 2020

Abstract

The presence of coronal holes in solar disk plays an important role in influencing the space weather and generation of the solar wind. As such there lies a requirement in proper study and prediction of coronal holes occurs in the solar disk. This, in turn, arises the necessity of detection of coronal holes present in the solar disk. In this work, a Hough transformed inspired fuzzy-energy simulated dual contours-based segmentation technique has been proposed for the detection and extraction of holes in solar disk. In the proposed method Hough transform has been induced to initialize the contour for the contour-based method of segmentation. In the algorithm, two contours (active and static) have been initiated and made to evolve based on the energy function by incorporating the gray-scale intensity. Here in the work one contour is made to deform its shape while the other contour is kept static for the coronal holes detection purpose. The experiment has been carried out on few benchmark datasets and the corresponding outcomes have been compared with the results of other existing algorithms. The comparison results highlight the performance of the proposed technique in detection of coronal holes in solar disk.
© 2020 COSPAR. Published by Elsevier Ltd. All rights reserved.

Keywords: Coronal holes; Solar disk; Hough transformation; Fuzzy energy; Active contour method; Fuzzy static contour

1. Introduction

Localization of solar coronal holes (CHs) is a major issue in the domain of solar physics. The low density regions in the solar corona which are visible as dark region due their lower density and temperature compared to the surrounding coronal plasma are considered as CHs (Munro and Withbroe, 1972; Rotter et al., 2012). The holes can occur during any stage of solar cycle, but it can be frequently observed during the declining stage of the solar cycle.

The solar CHs have a strong influence in the formation of high speed solar wind streams (HSSs) as-well-as in variation of space weather. This HSSs causes in geomagnetic storm during low solar activity[1], when the particles from these HSSs coinside with the Earth magnetic field (Rotter et al., 2012; Krieger et al., 1973; Gosling and Pizzo, 1999). These solar wind and geomagnetic storm has a strong impact on Earth's ionosphere. The high energy cloud generated as a result of solar wind get collide with Earth's magnetic fields, which in turn cause in changing the shape of the magnetic field. This in turn effects many electrical equipment as-well-as radio communications[2]. Along side it heat the Earth's outer atmosphere with energetic ultraviolet radiation, causing it to expand[3]. This causes reducing lifetime of Earth-orbiting satellites and

* Corresponding author.
E-mail addresses: sanmoy1985@rediffmail.com (S. Bandyopadhyay), saurabh.das@iiti.ac.in (S. Das), abhirup.datta@iiti.ac.in (A. Datta).

[1] https://www.sws.bom.gov.au/Educational/1/3/2.
[2] https://image.gsfc.nasa.gov/poetry/ask/a11534.html.
[3] https://hesperia.gsfc.nasa.gov/sftheory/spaceweather.htm.

https://doi.org/10.1016/j.asr.2020.02.012
0273-1177/© 2020 COSPAR. Published by Elsevier Ltd. All rights reserved.

also corrupt the accuracy of Global Positioning System (GPS) measurements. The geomagnetic storms is also responsible for electrical power interruption over a large region.

As such there rise a necessity of the statistical investigation of CHs mainly the effect of size, intensity level and location of holes for proper prediction of physical parameters of the solar wind and geomagnetic effects (Rotter et al., 2012). This in turn require the proper detection and extraction of CHs present in solar disk. In early days, CHs have been distinguished outwardly and physically followed by experienced eyewitnesses (Garton et al., 2018; Harvey and Recely, 2002). Recently, there have been a number of endeavors to robotize the method for the recognizable proof and discovery of CHs utilizing distinctive strategies. These methods are perimeter tracing (Kirk et al., 2009), intensity thresholding (Krista and Gallagher, 2009), fuzzy clustering (Barra et al., 2009), active contour method (ACM) (Boucheron et al., 2016), edge-based segmentation (Scholl and Habbal, 2009) etc. Among the different stated methodologies ACM is mostly preferred for image segmentation purpose due its capability to provide smooth and closed contours as an outcome of segmentation (Caselles et al., 1997). Moreover, the technique can achieve sub-pixel accuracy of object boundaries (Caselles et al., 1997). Alongside, the method does not require large datasets like CNN based segmentation technique for training and testing purpose. However, the contour based method suffer from the presence of blurred region boundaries. This lead to the misclassification of region of interest (RoI) present in the image. Moreover, the contour based method of CHs detection suffers from contour initialization problem, which often lead to the false detection of RoI (Boucheron et al., 2016; Chan and Vese, 2001). Apart from this, the single contour based techniques has a limitation that the contour get stuck in local minima and as such it unable to reach and detect proper region boundary (Chan and Vese, 2001; Bandyopadhyay, 2018; Meng et al., 2013; Gunn and Nixon, 1997).

Thus, in this work a new segmentation algorithm has been implemented for detection and extraction of the CHs in the extreme ultraviolet (EUV) solar disk images. For the purpose of CHs detection using segmentation algorithm, in this work a Hough transform inspired fuzzy energy-based dual contours model has been proposed. In the proposed technique Hough transform algorithm has been induced for the contours initialization, which is the first step of the contour based algorithm. In this work two contours, namely; active contour and static contour has been generated for the overall segmentation purpose. Here, the active contour has been initialized with a view to segment the solar-image based on fuzzy energy-based active contour method (FEACM) (Krinidis and Chatzis, 2009). In later stage fuzzy static contour (FSC) has been initiated to extract CHs regions from the segmented image. Based on the final position of the contours the holes are detected. Thus the main contribution in this work is;

- The implementation of fuzzy energy-based dual contour method (FEDCM) for detection of CHs in solar image.

The proposed algorithm has been tested on solar image benchmark datasets taken for a single year (one image per day) and the corresponding results have been compared with the output from other existing algorithms for proper validation of the proposed work of CHs detection.

The organization of this article goes as follows. The discussion on related works have been done in Section 2. In Section 3 the proposed work has been explained. Discussion on obtained results has been stated in Section 4. Finally, in Section 5 the overall conclusions on the proposed work has been drawn.

2. Related work

There exists two major issues which are associated with the detection of CHs in solar disk image. These issues are solar limb correction and segmentation of solar image respectively. Several strategies had been used to handle these problems.

2.1. Solar limb correction

Solar limb correction or off-disk region (region consists of solar-limbs and solar image background) elimination is an important steps in order to obtain accurate CHs segmentation results. Limb brightening correction was first proposed by Barra et al., 2009, where a polar transform was applied to transform the image into polar plane with the origin at the solar disk center. Reiss et al. (2015) had implemented limb brightening correction by introducing smooth transition function followed by inverting the output. Afterward, the authors had applied a square-root transformation on the inverted image (Reiss et al., 2015). A prior solar disk segmentation was carried out by Illarionov and Tlatov (2018), where maximal intensity value was rewarded for the off-disk pixels. A preprocessing step had also been applied where all off-disk pixels are removed by rewarding them with similar intensity value (Delouille et al., 2018). In the work (Nieniewski, 2004), a two white color ring has been setup; one, on the solar disk boundary and another on the solar limb, using Bresenham algorithm (Bresenham, 1965). Afterward, using image dilation operation region inside the circles was filled and smoothed, in order to eliminate the problem occuring due to limb effect and presence of off-disk region. Boucheron et al. (2016) had generated circular mask based on the data provided in solar image *fits* file. However, most of the techniques has to depend on exact information about the center pixel co-ordinates positions of solar disk and solar radius, $R_{\odot}$.

2.2. Coronal holes segmentation

Krista and Gallagher (2009) had made utilize automated image segmentation technique for detection and extraction of holes. For the purpose intensity thresholding technique

had been used. The thresholding technique was tested on EUV and 195 Å or X-ray images. In the work, the full-disk images were converted into Lambert equal-area projection maps and partitioned into a series of overlapping sub-images (Krista and Gallagher, 2009). From this converted and partitioned images local histograms were extracted. Based on this obtained histogram the threshold value had been determined. This threshold value were then used to classify CHs. However there lies a limitation in the method. This limitation occur due to near-limb effects. These near-limb effects lead to the inability to determine a dominant polarity, incorrect boundary determination, and incorrect area determination (Krista and Gallagher, 2009).

Spatial possibilistic clustering algorithm (SPoCA) had been introduced by Barra et al. (2009) in order to segment solar EUV images and to detect the CHs present in the images. The algorithm consists of multi-channel unsupervised spatially-constrained fuzzy clustering method, which had been used for segmenting EUV images into regions of interest. In order to improve the accuracy of segmented output few parameters and techniques had been embedded with SPoCA, which incorporate steps like limb correction, sursegmentation and optimal clustering, and sensor data fusion process. The improved algorithm has the capability to decompose the whole set of extreme ultraviolet telescope (EIT) solar images over the 23rd solar cycle into regions which in turn can clearly be classified as coronal hole, quiet sun and active region. But, the filament channels observed in coronal EUV passbands are often misclassified as "CHs" in the segmentation procedure (Barra et al., 2009).

The coronal hole identification via multi-thermal emission recognition algorithm (CHIMERA) had been implemented by Garton et al. (2018), which considers multi-thermal images from the atmospheric image assembly (AIA) onboard the solar dynamics observatory (SDO) (Lemen et al., 2012) for segmentation of CHs boundaries. The method segment out the CHs by analyzing the intensity ratio of multi-thermal images across three passbands namely; 171 Å, 193 Å and 211 Å, and one simultaneous snapshot from the helioseismic and magnetic imager (HMI). CHIMERA allows accurate segmentation of CH boundaries and many of their properties, such as area, latitudinal and longitudinal width, position, and magnetic polarity of extracted CHs. However, the method has a limitation in classification of partially or fully occulted CHs arise due to occultation from brighter features. These lead to errors in segmentation of CHs boundary and the estimation of near-limb CHs properties (Garton et al., 2018).

Verbeeck et al. (2014) had introduced modified spatial possibilistic clustering algorithm (SPoCA) suite for detection of active region (AR), coronal hole (CH) and quiet Sun (QS) regions in coronal image. The method is not only applicable on EIT images, it can be also used for handling EUVI, SWAP, and AIA images with an additional tailored algorithm for each. The modified SPoCA suite incorporates three different kinds of fuzzy clustering algorithms. These are specially tailored to the segmentation of solar coronal in EUV images (Verbeeck et al., 2014). The used fuzzy algorithms are, SPoCA that uses neighboring intensity values, the fuzzy C-means (FCM), and a regularized version of FCM, which is also known as possibilistic C-means (PCM) algorithm. Moreover, the algorithm require a few preprocessing steps to get an accurate segmentation of EUV images.

Nieniewski (2004) as-well-as Ciecholewski (2015) have implemented the combined algorithms of watershed transform and region merging based technique for segmentation of CHs from solar disk image. In Nieniewski (2004) author used EIT image for the detection of CHs. The authors had down-sampled the original image size to 512×512 for reducing the computational time requirement by the algorithm. The maximum iterations taken by the technique proposed by Nieniewski (2004) was found to be around 180. Ciecholewski (2015) in his work had used EIT 195 Å wavelength images with the resolution of 1024×1024 for extraction of CHs from the solar disk region. Unlike the CHs detection method as described in Nieniewski (2004), in Ciecholewski (2015) the author has considered only the inside area which is obtained after circumscribing using a superposed ring.

In Scholl and Habbal (2009), the authors had worked with three sets of EUV EIT images, namely 171 Å, 195 Å and 304 Å wavelength images. For the purpose of detection of holes and other regions in the images different image processing steps have been applied in work. Where, the authors had used histogram based and region growing based segmentation method for the extraction of features in the images and in the later stage of the work combination of both region based and edge based methodologies had been applied for extraction of region of interest from the corresponding images. The method requires visually distinguishable features in higher spatial resolution for the automated detection of CHs and filaments more accurately.

Illarionov and Tlatov (2018) have used convolutional neural network (CNN) based image segmentation technique for extraction of CHs regions from solar disk image. The authors in this work have used one CHs segmentation map image (obtained from Kislovodsk Mountain Astronomical Station of the Pulkovo Observatory[4]) per day covering the time period from 2010 to 2018, in 1024×1014 resolution to train the network. Along side, the authors have used SDO/AIA images processed by LMSAL[5] for training and testing the neural network. The technique involves random transformation in preprocessing steps of training of neural network. This require large number of datasets for training purpose. Total, 2916 pairs of solar disk images have been used in the experiment, where 2898 images have been used for training and testing

[4] http://en.solarstation.ru/.
[5] http://suntoday.lmsal.com/suntoday/.

purpose. Moreover, in the preprocessing step image size has been reduced to the resolution of 256×256.

Detection of CHs had also been performed using active contour method by Boucheron et al. (2016). In the work the authors had applied Chan-Vese model of active contour without edge (ACWE) (Chan and Vese, 2001) on 193 Å images of AIA level 1 datasets from four different time span, accessed from the Joint Science Operation Center (JSOC)[6]. Contour initialization is a major issue which is associated with this type of contour based segmentation. Accuracy of image segmentation using contour based method rely on procreation of initial contour. Usually for accurate RoI detection, the contour is assigned within the RoI (Wang et al., 2017; Darolti et al., 2008; Xingfei and Tian, 2002; Huang and Zeng, 2015). This strait of contour initialization require human guidance as-well-as prior information about RoI location. Different strategies such as initializing contour near the image boundary, outside RoI, as-well-as contour initialization free ACM had been introduced to overcome this problem of contour initialization within the object boundary (Chan and Vese, 2001; Xie and Mirmehdi, 2010). However, due to the presence of off-disk region in solar image, these types of contour initialization may also rise a problem. Since, the contour has a tendency to stuck at local minima, so, there lies a high probability for a contour to stuck on the boundary of solar-limb and misclassify the regions. Alongside, the background region in solar disk images having same color composition as that of the CHs regions, so there lies a higher chance that both the regions in solar disk images get classified as the RoI. In Boucheron et al. (2016), the authors had initialized the contour by thresholding at a low intensity that is firm to lie within the CHs region. This initialize contour get evolve according to the energy function of the ACWE and after predefined condition it get stuck on the boundary of the CHs regions. The center co-ordinate points and solar disk radius data provided by the solar *fits* file plays a vital role in evolution of the contour. In the work Boucheron et al. (2016) reduce the resolution of the image decimated by $8\times$ in order to speedup the computation.

3. Proposed work

CHs are most effectively experienced in space-based X-ray and EUV images. The regions are observed as dark areas in the solar corona in these images. The holes become apparent as dark region since they are cooler, less thick segments than the encompassing plasma and are segment of open, unipolar magnetic region[7]. Thus the detection of CHs in solar image can easily be transformed into the problem of detection of darker region (generally black portion with low intensity level) in the image. Mapping the shape of CHs is kind of like attempting to degree the edge of a cloud – it is simple to determine what is certainly a holes and what isn't, but the boundary is fuzzy and diverse eyewitnesses will stamp the edge in an unexpected way[8]. The things become complicated when, CHs show up differently in different wavelengths. The shape, size and darkness of any observed holes are not steady between different watching channels. Moreover, the data provided by an EUV solar image is ambiguous. It consists of readout and Poisson noise, as-well-as cosmic ray hits. This presence of noise causes local minima and maxima in the image brightness function (Nieniewski, 2004). Alongside, it suffer from observational biases and is subject to interpretation (Barra et al., 2009).

In order to overcome the above mentioned problem of contour initialization as-well-as solar limb correction and to detect the CHs region accurately in the work a novel fuzzy energy-based dual contours method (FEDCM) has been proposed. For performing the task of CHs detection using FEDCM, here in the work an advanced and modified version of FEACM has been implemented. The term dual contours has been in this work since, in the work two contours have been initialize simultaneously. Here the one contour has been initialized to focus on segmentation of solar image, while, the other contour initialized, used for extraction of CHs from segmented image. The proposed algorithm has been segmented into three phases. In the first phase of the work, circular Hough transform has been introduced for initialization of the initial contours for FEDCM technique. FEACM has been incorporated for segmentation of solar image, in the second phase. At-last in the final phase, FSC has been induced to extract out the CHs regions from the segmented solar image.

3.1. Contour initialization using circular Hough transform

With a view to tackle the problems of initial contour generation and presence of off-disk region, respectively. both in the domain of contour based image segmentation and CHs detection, in this work, circular Hough transform simulated contours initialization has been proposed. This has been done, keeping in view the fact that, the solar disk in solar image is circular in shape and the region of interest is situated within the solar disk. Circular Hough transform, a pattern recognition technique, which Duda and Hart (Jan. 1972) had used for detection of circular shaped object in noisy and imperfect image by voting procedure (Hough, 1962). A brief about circular Hough transform technique used for contour initialization is given in Appendix A.

3.2. Solar image segmentation using FEACM

After the initialization of the two contours ϕ_1 and ϕ_2 using circular Hough transform, one contour ϕ_2, has been

[6] http://jsoc.stanford.edu/.

[7] https://www.swpc.noaa.gov/phenomena/coronal-holes.

[8] http://blog.aurorasaurus.org/?p=437.

kept static, while the other contour ϕ_1, is made to evolve base on FEACM. FEACM is inherently the fuzzified version of the Chan-Vese ACM developed by Krinidis and Chatzis (2009) for the purpose of image segmentation. The model has capability to detect objects with ambiguous boundaries or objects whose border are not constrainedly presented by gradient. This FEACM used fuzzy energy in order evolve the initialize contour. The contours stop evolving after reaching at the object boundaries present in the image, based on predefined criteria. This predefined criteria is set on total energy obtained from the optimization function. If the total energy of the fitting function remain unchanged compared to the energy obtained in previous iteration, the curve will stop deforming further and the position where the contour get stuck is considered as the boundaries of RoI. As such, the region inside the curve is contemplated as the desired object present in the image.

In problems of contour evolution, the level set method and in definite the motion by mean curvature introduced by Osher and Sethian (1988) have been implemented in particular, since it permits for corners, cusps, and spontsneous topological changes (Chan and Vese, 2001). Additionally, the discretization of the issue is made on a settled rectangular lattice. The contour is denoted completely through a Lipschitz function ϕ_1, by $C = \{(x,y)|\phi_1(x,y) = 0\}$, and the advancement of the contour is given by the zero-level curve at time t of the function $\phi_1(t,x,y)$.

Definition 1 (*Lipschitz functions*). For a given image $I : \Omega \longrightarrow \mathbb{R}$ the function $\phi_1(t,x,y) : \Omega \longrightarrow \mathbb{R}$ is said to be Lipschitz function if there exists a constant L such that $|\phi_1(t,x_1,y_1) - \phi_1(t,x_2,y_2)| \leqslant L|(t,x_1,y_1) - (t,x_2,y_2)|$ for all $x, y \in \mathbb{R}$. Where, $\Omega \subset \mathbb{R}^2$ is the image domain. The smallest constant $L$for which this inequality holds is called the Lipschitz constant of $\phi_1(t,x,y)$, denoted by $L(\phi_1(t,x,y))$ (Wang and He, 2012; Poria et al., 2017; Luxburg and Bousquet, 2004).

In FEACM based on the curve C formed using circular Hough transformation in image domain Ω, the initial formulation for the curve at time $t = 0$, is given by;

$$\phi_{10}(x,y) = \phi_1(0,x,y) = \sqrt{(x-a)^2 + (y-b)^2} - r. \quad (1)$$

Now, for FEACM a pseudo level set formulation, which is denoted similar to the level set method (Osher and Sethian, 1988), based on the membership values u, where $C \subset I$ is expressed by the pseudo zero level set of Lipschitz function $u : I \longrightarrow \Omega$, such that:

$$u(x,y) = \begin{cases} > 0.5 : if\ (x,y)\ is\ inside\ C, \\ = 0.5 : if\ (x,y)\ is\ on\ C, \\ < 0.5 : if\ (x,y)\ is\ outside\ C. \end{cases} \quad (2)$$

The same hold true for the case of circular contour ϕ_2.

Based upon the formulation given in Eq. (1), the image $I$is partitioned into two regions of approximately homogeneous intensities, of different values I^i and I^o. Where $I \approx I^i$ represents region inside the contour C and $I \approx I^o$ represents region outside the contour C. As, shown in Fig. 1.

Now, flourished on this concept the initial energy function for the curve has been given by Krinidis and Chatzis (2009),

$$F_1(C) + F_2(C) = \int_\Omega [u(x,y)]^m |I(x,y) - c_1|^2 dxdy + \int_\Omega [1 - u(x,y)]^m |I(x,y) - c_2|^2 dxdy. \quad (3)$$

where, the fuzzy membership function $u(x,y) \in [0,1]$, and m is a weighting exponent on each fuzzy membership (Krinidis and Chatzis, 2009).

Ultimately, the fitting term or the initial energy function given in Eq. (3) attends its minimum value when $C = C_0$, i.e., when the contour Cconverges on the boundary of the RoI. That is,

$$\inf_C\{F_1(C) + F_2(C)\} \approx 0 \approx F_1(C_0) + F_2(C_0). \quad (4)$$

The FEACM is based on the fuzzy energy minimization, which can be noted as a specific case of a minimal segment issue. The model minimize the energy function stated in Eq. (3), taking into consideration, an additional length term of the model C as a regularization descriptor. Thus, the optimization functional has been introduced as (Krinidis and Chatzis, 2009):

$$F(C,c1,c2,u) = \mu.Length(C) + \lambda_1 \int_\Omega [u(x,y)]^m |I(x,y) - c_1|^2 dxdy + \lambda_2 \times \int_\Omega [1 - u(x,y)]^m |I(x,y) - c_2|^2 dxdy, \quad (5)$$

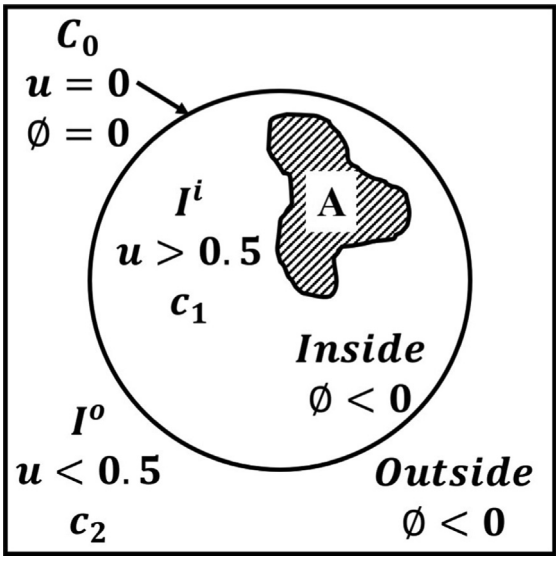

Fig. 1. Diagram representing initial contour position, object **A**, fuzzy membership value assigned and average pixels intensities inside and outside the curve.

where, μ represents the weight factor for the curve length and the terms λ_1 and λ_2 denotes the weight values assigned for foreground consistency and background consistency respectively. Detail notion about the parameters used and numerical approximation is given in Appendix B.

The major advantage of this FEACM is that, the method has the combined advantage of both ACM and fuzzy clustering technique as discussed in Krinidis and Chatzis (2009). The ACM has the ability to handle topological changes of contour curves (Chan and Vese, 2001; Fang et al., 2019). On the other hand, the calculation of c_1 and c_2 in FEACM is based on soft clustering technique. This allows gradual memberships of pixels to clusters measured as degrees in [0,1]. This gives the flexibility to express that pixels can belong to more than one cluster (Bora et al., 2014). This in turn leads to robust and accurate pixel clustering. Moreover, the fuzziness of energy yields a adjusted strategy with a strong capability to overcome "weak" local minima. As such, it reduce the probability of misclassification. Furthermore, the FEACM shows its promises in tackling the noisy images (Krinidis and Chatzis, 2009). Along side, the method approach towards the desired object contour very quickly, since it does not encounter the Euler-Lagrange equations of the classical contour based problem, but, instead, enumerate the fuzzy energy changes directly (Krinidis and Chatzis, 2009).

3.3. Extraction of CHs using FSC

However, in this case of FEACM based segmentation, the method will segment solar image in such a way that, it will level low intensity regions (background of the solar image and CHs regions) as background pixels. On the other hand, solar limbs and non-CHs regions of solar disk will be level as foreground pixels in the image. As such, all the foreground pixels in segmented image will assign with the membership value $u(x,y) > 0.5$, and membership value $u(x,y) < 0.5$ will be assigned to the background pixels.

Thus, in order to handle the stated situation of misclassification and eliminate the off-disk regions, in this work FSC has been introduced. The contour has been named static contour due to non deformation of the contour shape throughout the task, i.e., the contour remain static during whole process of CHs extraction. The implementation of FSC for solar CHs, has been done by keeping three points in view. First, the CHs regions are not present in the off-disk region, second, any object detection algorithm in image processing domain has the probability to misclassify RoI, and third, both background and CHs regions in the used solar image are having same color intensity.

Now, in order to extract out only CHs region from the segmented image, a fuzzy rule base are formed based on the final membership values obtained during the segmentation and membership values generated due to the FSC for the contour ϕ_2. Three rules formed in fuzzy rule base are mentioned as follows:

- If $u(x,y)_F > 0.5$ and $u(x,y)_S < 0.5$, set (x,y) as background, i.e., $u(x,y)_{New} < 0.5$.
- If $u(x,y)_F > 0.5$ and $u(x,y)_S > 0.5$, set (x,y) as background, i.e., $u(x,y)_{New} < 0.5$.
- If $u(x,y)_F < 0.5$ and $u(x,y)_S > 0.5$, set (x,y) as foreground CHs regions, i.e., $u(x,y)_{New} > 0.5$.

Where the terms $u(x,y)_F, u(x,y)_S$ and $u(x,y)_{New}$ represent the membership values obtained as final output using FEACM, FSC, and the new rules formed respectively. Flourished on these three stated rule CHs regions are extracted out from the segmented image based on FEACM. As, shown in Fig. 2. The fundamental advantage of using FSC is that the method does not depend upon SDO metadata seperately like other existing algorithm of

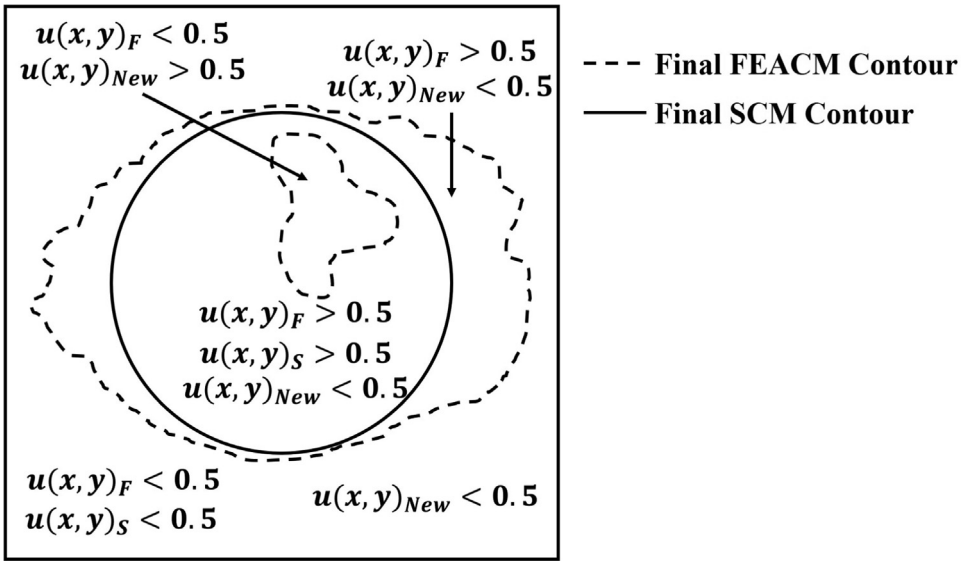

Fig. 2. Diagram representing membership values obtained as final output using FEACM, FSC, and the rules formed respectively.

CHs segmentation for, solar disk center and radius values to initialize contour and overcome the limb effect in solar disk image. Hence, the method can be applied on any type of solar disk image.

The corresponding algorithm of the introduced CHs segmentation has been given in Appendix C. The related block diagram is given in Appendix D.

4. Results and discussion

4.1. Datasets

For the experiment in this work the solar disk images of size 1024×1024 has been used. The images is of SDO/AIA which has been observed by the Solar Dynamics Observatory (SDO) with the Atmosperic Imaging Assembly (AIA), and has been collected from Solar Dynamics Observatory (SDO)[9]. SDO contains images of 10 different wavelengths, measured in angstroms Å, captured with its AIA instrument module at an interval of every ten to twelve seconds (Kucuk et al., 2017). AIA generally capture images in multiple EUV and ultraviolet (UV) pass bands[10]. In this work, one EUV band pass image per day for the year 2017 are used in the experiment to detect CHs have been observed by optimizing four AIA telescopes centered on the specific line of 193 Å. The solar image in this wavelength is typically colorized in light brown[11]. In the EUV images brighter regions represent hot active regions, solar flares, and coronal mass ejections[12]. As stated earlier in Section 3, the dark areas indicates CHs where very little radiation is emitted.

4.2. Parameters settings

The contour has been evolved based on four parameters. These are, μ, m, λ_1 and λ_2. The weight parameter for length of the curve μ has been kept at 0, with a view to reduce the complexity of the fitting function. Also it is a fact if the value of μ set low, then the contour has the probability to detect small disjoined regions present in the images. The term m, weighting component of the fuzzy membership, has been awarded with weight of 20in order to handle the fuzziness of a pixels at a particular location in the image. If the value of m is kept in higher, then the fuzziness associated the pixels will be high. A experiment has been conducted to fixed up the value for the parameters λ_1 and λ_2. Heuristic approach has been taken for the purpose, using which an intermediate values have been setup for the parameters λ_1 and λ_2. The parameter λ_1 is assigned with value of 0.5 and the notion λ_2 is awarded with value 0.1. Values of λ_1 and λ_2 has been chosen in such a way so that a there should remain a proper balance between foreground and background pixels. Otherwise, there is high chance the coronal hole pixels to get classified as a non-coronal hole pixels and vice versa. The experiments carried out for determination of the proper parameters value. Where the proposed algorithm has been applied on SDO/AIA image tested for different values of μ, m, λ_1 and λ_2 for selection of optimal value of the parameters, which has been shown in the Fig. 3.

4.3. Comparison with other methods

The work has been carried out using SDO/AIA 193 Å images taken for year 2017. One solar image per day has been picked up for the stated period. The proposed method of circular Hough transformed inspired FEDCM has been applied on the mentioned datasets. Corresponding output obtained after applying the proposed method have been shown in the last column of the Figs. 4 and 5.

Presently there are several constrain which are becoming barrier in the comparison of CHs detection algorithms (Boucheron et al., 2016). Firstly, progressing algorithmic alterations for numerous of the commonly utilized strategies make it troublesome for any single agent to be certain they are utilizing the foremost later algorithm. Secondly, usage for algorithms are not continuously freely accessible and may not be in a unreservedly accessible freely. Thirdly, there is lack of proper ground truth for the comparison purpose (Illarionov and Tlatov, 2018).

Inspite of the stated barriers, in order to validate the performance of the proposed algorithm, the output of the proposed FEDCM[13] has been compared with the results obtained using ACWE method of segmentation (ACWE Seg)[14], CNN based segmentation (CNN Seg)[15], CHIMERA[16] and SPoCA[17], with respect to ground-truth generated flourished on the synoptic map image[18] (SM-GT) and CHs segmentation map[19] (RG-GT) (shown in second and third column of the Figs. 4 and 5 respectively). Synoptic maps (as shown in Figs. 7b and 8b) of the solar disk image is basically a snapshot of the various features of the Sun created by the SWPC forecasters for each day by drawing the various phenomena of the Sun they observe. This map is an important tool for assessing the conditions on the Sun and predicting the appropriate forecast based on these observed conditions. It provide the forecasters, a broad outline of solar surface features, such as; neutral lines, active regions, coronal hole bound-

[9] https://sdo.gsfc.nasa.gov/.
[10] https://aia.lmsal.com/public/instrument.htm.
[11] https://www.nasa.gov/content/goddard/how-sdo-sees-the-sun.
[12] https://astronomy.stackexchange.com/questions/24010/whats-the-rationale-behind-the-false-colours-in-solar-observation-photographs.
[13] https://github.com/sanmoy1985/CoronalHolesFuzzyContour.
[14] The corresponding source code can be available from the author on personal request.
[15] https://github.com/observethesun/coronal_holes.
[16] https://github.com/GartontT/CHIMERA.
[17] https://docs.sunpy.org/en/stable/generated/gallery/plotting/overplot_hek_polygon.html.
[18] https://www.swpc.noaa.gov/products/solar-synoptic-map.
[19] https://github.com/observethesun/coronal_holes/tree/master/data.

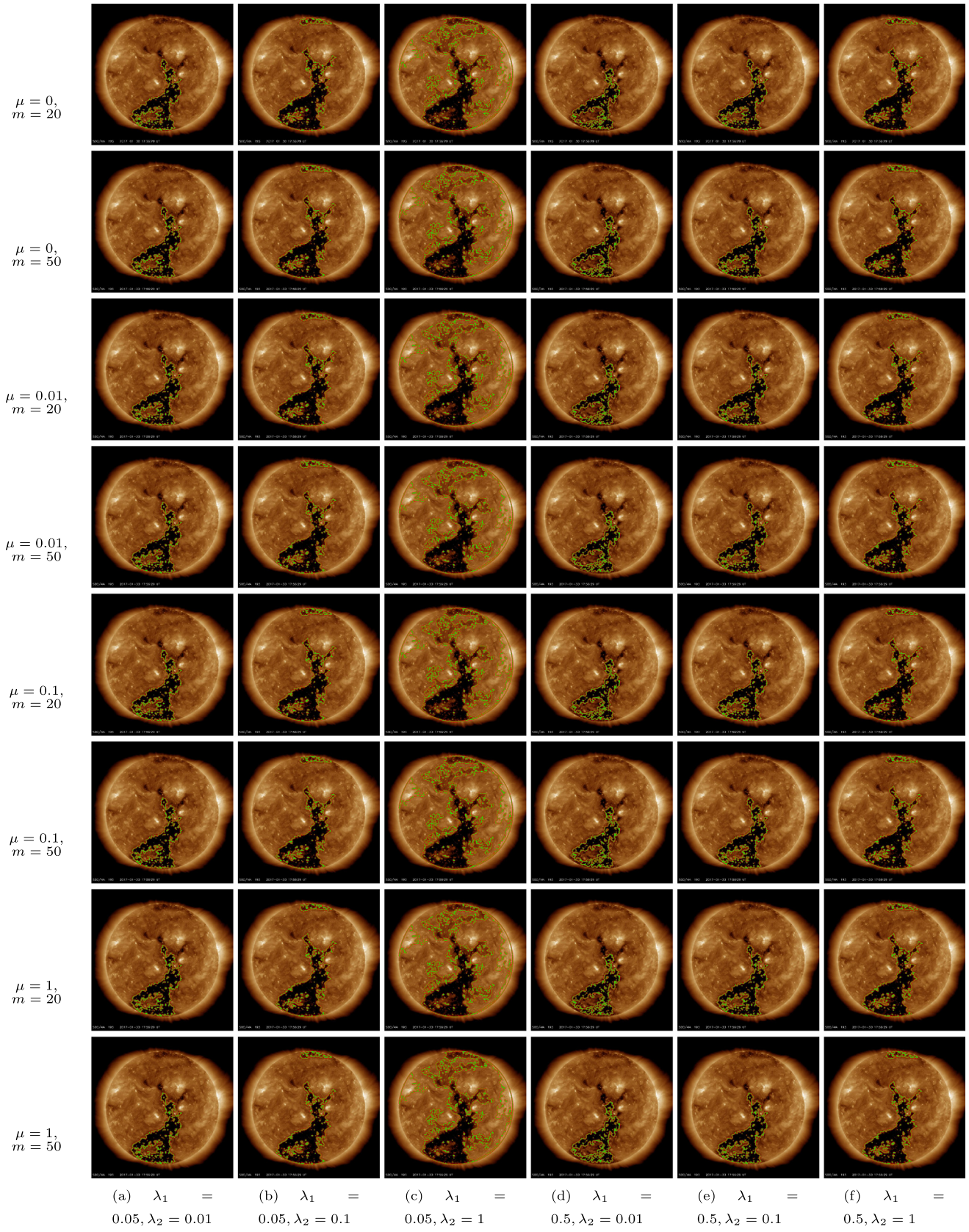

Fig. 3. A heuristic approach to test the performance of proposed FEDACM on SDO/AIA solar image of 193 Å wavelength captured on 2017-01-30, for different parameters value.

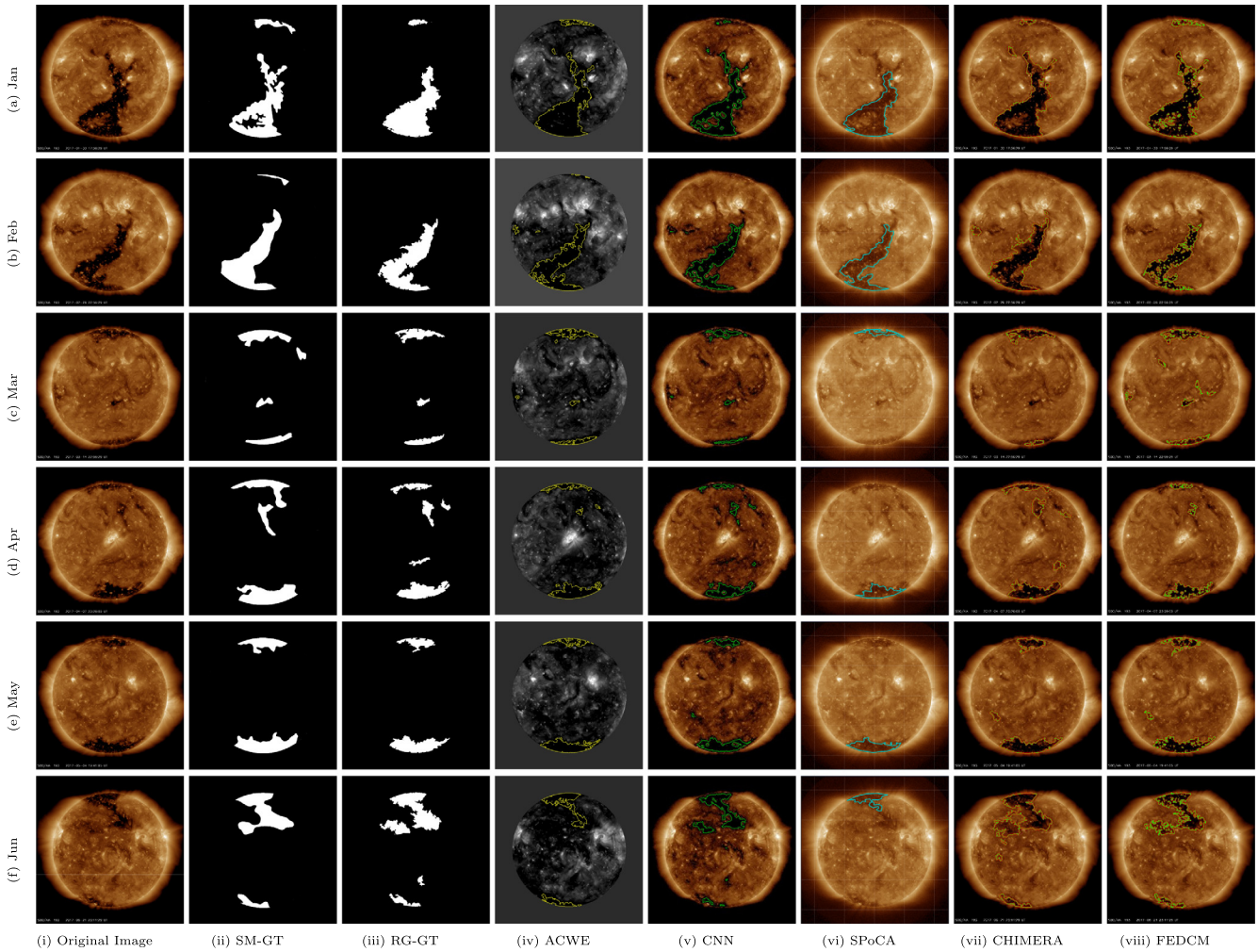

Fig. 4. A pictorial summarization showing Original Image in (i) followed by ground-truth images in (ii) and (iii), and results obtained using ACWE Seg, CNN Seg, SPoCA, CHIMERA and the proposed method in (iv)–(viii) respectively, for the period of Jan–Jun.

aries, filaments, plages, and prominences. The synoptic maps also contain information about list active region numbers, coronal hole polarity, and have proton and flare event probabilities for each region. These maps have been produced daily since 1972. On the other hand CHs segmentation map has been generated using the region growth image segmentation algorithm which can be obtained on daily basis from Kislovodsk Mountain Astronomical Station.

The comparison has been carried out in terms of visual observation, segmentation matrix, execution time and the astrophysical parameters predicted based on the CHs regions detected in the solar image. The comparative results have been shown in Figs. 4 and 5. One solar image per month have been considered for the comparison purpose, in this work.

4.4. Visual analysis

The original solar image and corresponding outputs used for comparison purpose have been highlighted in Figs. 4 and 5. In the Figs. 4 and 5, the first column contain the original image used for the detection of CHs. The ground-truth image SM-GT and RG-GT, and the outputs obtained after the application of ACWE Seg, CNN Seg, SPoCA and CHIMERA based CHs detection have been shown from second to seventh column in the figures respectively, and corresponding output obtained using FEDCM have been shown in the last column of the figures.

Based on visual analysis of the output shown in the last column of the Fig. 4a and ground-truth image displayed in the second column of the Fig. 4a, it can be concluded that the proposed method has outperform compared to other methods. The proposed method has detected exact CHs boundary along with the non-coronal hole regions present within the coronal hole region in solar image given in Fig. 4a. While the ACWE based segmentation technique as-well-as CHIMERA has misclassified the non-coronal hole region as CHs. At the same time, it can be seen that CHs contour generated based on the CNN technique and SPoCA, is far away from the existing CHs boundary. Moreover, CNN based technique has failed to detect the coronal hole region present in the upper portion of the solar disk properly, which has been detected by both

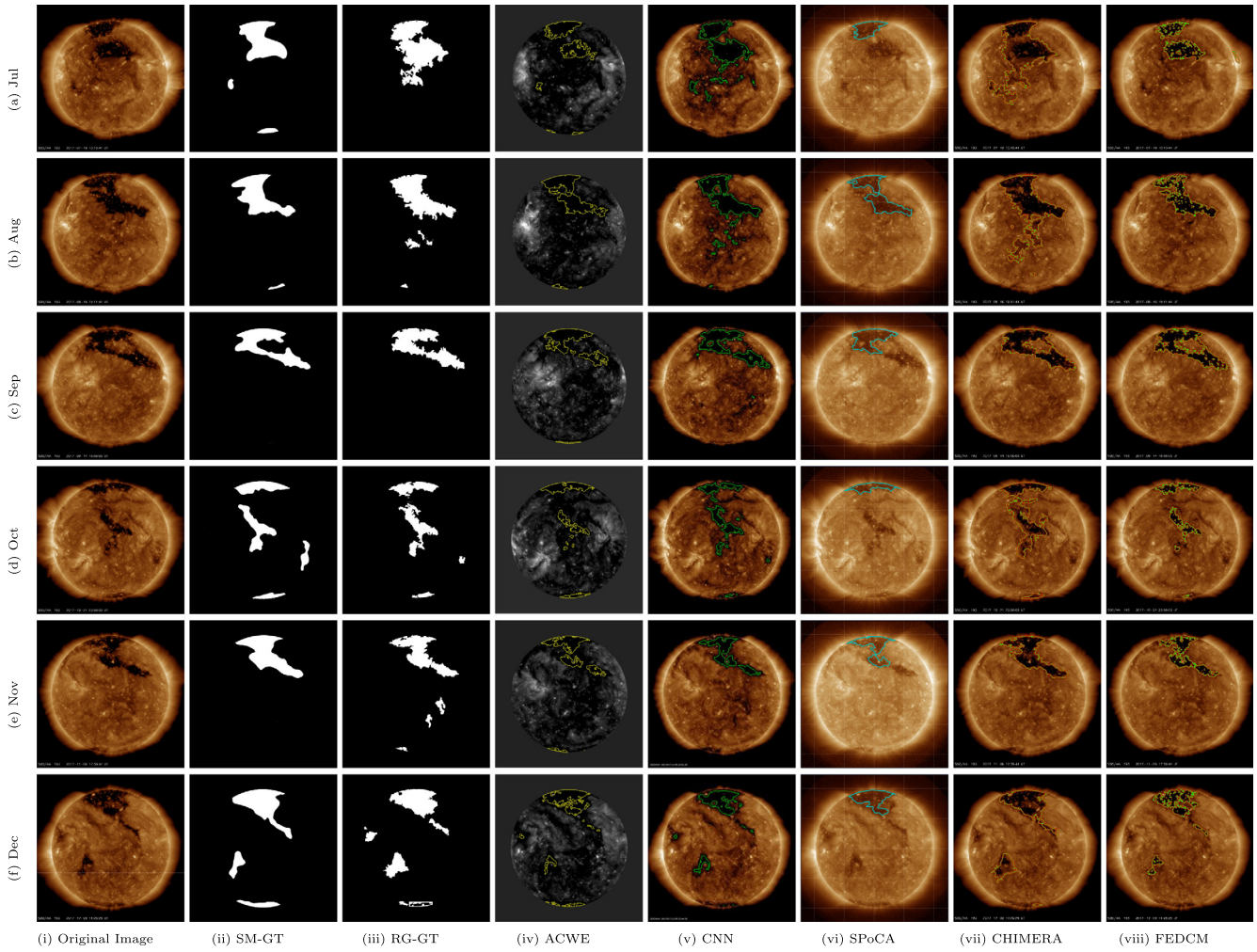

Fig. 5. A pictorial summarization showing Original Image in (i) followed by ground-truth images in (ii) and (iii), and results obtained using ACWE Seg, CNN Seg, SPoCA, CHIMERA and the proposed method in (iv)–(viii) respectively, for the period of Jul–Dec.

ACWE and proposed FEDCM method. However, while comparing outputs with the ground truth image given in the third column of Fig. 4a, it can be concluded that ACWE, CNN and SPoCA techniques have generated more-or-less same outputs, while CHIMERA and FEDCM has covered extra region.

Now, for the output image displayed in Fig. 4b, it can be visualized that for this case, the contour generated by CNN based technique, ACWE method of CHs segmentation and FEDCM technique have able to set the contour on the boundary of the CHs. But, both ACWE and FEDCM have detected few portion of the image as non-CHs regions, which has not been shown in the SM-GT. However, if the brightened and magnified image of that particular portion is taken in account (shown in Fig. 6), it can be easily noticed that, in original solar image taken on *Feb*, there exist a non-coronal hole region which has been detected by the contour based technique. Now, while comparing the performance of both the contour based technique, founded on the images shown in fourth and last column of the Fig. 4b and image displayed in Fig. 6, it can be easily stated that the proposed method has extracted out most part of the non-coronal hole region from the image compared to the ACWE method. This is due to the fact that, the formulation of energy function for the proposed technique is based on the intensity level of the image pixels under consideration. This energy function finally, segment image into two piecewise-constant distinct regions based on fuzzy approximation of intensities. Thus, the proposed technique efficiently partition the solar image into two regions namely; CHs (darker) and non-CHs (brighter) regions based on the intensity values. As such, the technique can easily separate out brighter points (pixels with higher intensity value) from that of the CHs points (pixels with lower intensity value). On the other hand, the misperformance of ACWE based CHs segmentation method is due to the fact that, the method perform on the low resolution image. Thus, while downgrading the original image of size 4096×4096 to low resolution image of size 512×512 some important pixels in the image which contain information about the RoI get erased. As such, there is an information loss take place in the low resolution

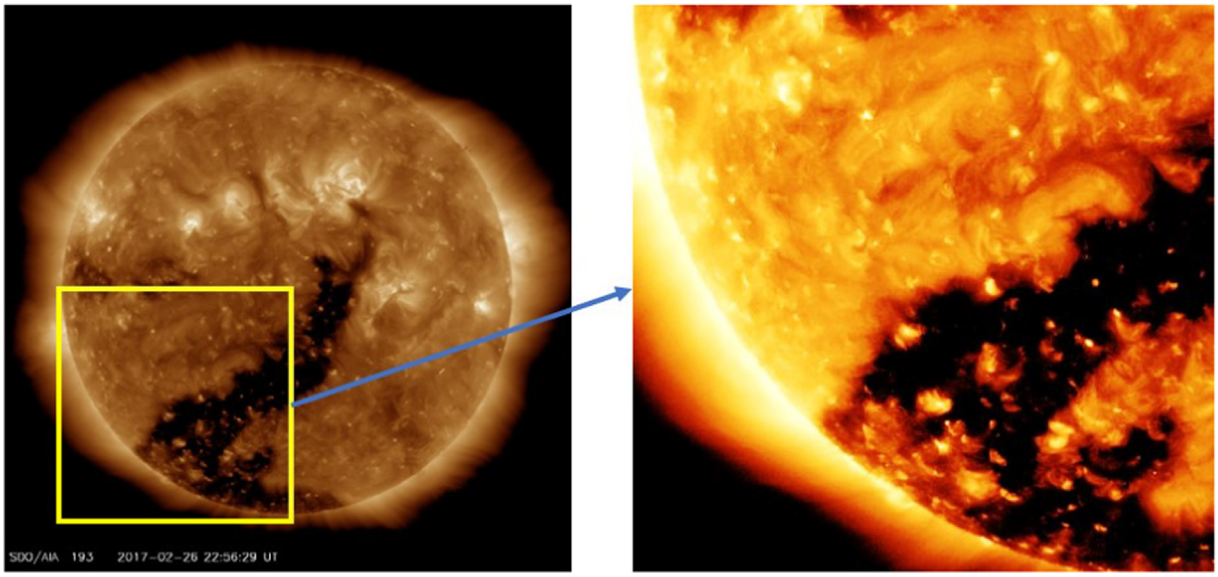

Fig. 6. Brightened and enlarge image of a portion of solar image taken on *Feb*.

image. At the same time, for the case of SPoCA and CHIMERA it can be concluded easily that the methods have under-segment and over-segment the solar image respectively.

From the output image shown in last column and second last column of the Fig. 5c, it can be visually analyze that the proposed method and CHIMERA have outperform better compare to the other existing method of CHs segmentation. In all the output obtained using ACWE, CNN and SPoCA, it can be noticed that contour obtained using these methods unable to reach the desired region boundary. While on the other hand it can be found that the final curve generated using the FEDCM able to detect the exact region boundary, same as highlighted in SM-GT taken on *Sep*. However, the FEDCM has detected few non-CHs region present within the CHs this is due to the virtue of FEACM.

However, for case of few solar image data such as solar images captured on *Nov*, *Dec* (displayed in Figs. 5e and f) it can be noticed that the FEDCM method fail to detect exact boundary of the CHs region. The final contour get stuck well before the CHs region boundary. This may occur due to two reasons; firstly, single contour based FEACM technique used for initial segmentation of the solar image has a general tendency to stuck at the local minima of the image, secondly, parameters involved in the fitting function plays a vital role in deformation of the curve and force the curve to move towards the boundary of RoI, and these parameters value sometimes fails if some variation present in the image features. Also, if these parameter are not properly chosen then there lies a high probability that, the curve stop deforming well before reaching the desired region boundary.

Moreover, it can also be visualize from the output images that the proposed technique has detected many small region inside CHs. This may be due to the fact that, actually there may be some existence of small non-CHs region inside the boundary of the CHs region, which can also be noticed from enlarge and brightened image displayed in Fig. 6, which the other existing method of CHs detection fail to detect. This misclassification can take place either due to the incapability of the existing algorithms used for CHs detection, or due to downgrading the image to low resolution for faster execution of existing algorithms, like ACWE and CNN. However, the proposed FEDCM work on image with original resolution and has capability to detect small topological change present in the image, along side the method has advantage to identify the object with vague boundary.

4.5. Quantitative analysis

The performance of the introduced technique has also been analyze quantitatively in terms of segmentation matrix, and has been compared with other existing algorithm of CHs segmentation. The segmentation matrix has been calculated with respect to the ground-truth image generated from the synoptic map and the image generated from region growing based CHs segmentation map. Two segmentation metrics namely; dice coefficient and Jaccard index. Both the metrics are used for the measurement of similarity coefficient between finite sample sets. The dice coefficient (D_C) and Jaccard index (J_{In}) are represented by;

$$D_C = \frac{2|A \bigcap B|}{|A| + |B|}, \tag{6}$$

and

$$J_{In} = \frac{D_C}{2 - D_C} = \frac{|A \bigcap B|}{|A| + |B| - |A \bigcap B|} = \frac{|A \bigcap B|}{|A \bigcup B|} \tag{7}$$

respectively. Where, the term A denotes the ground-truth of solar image and B represents output image or region inside the final curve. The main difference between Jaccard index and dice coefficient is that, the Jaccard index counts true positives (if the instance is positive and it is predicted as positive, it is counted as a true positive) only once in both the numerator and denominator. Better performance of the segmentation algorithm is reflected by higher value of dice coefficient and Jaccard index.

From the segmentation metrics of the existing algorithms and the proposed method highlighted in Table 1, and figures displayed in Figs. 4 and 5, it can be easily stated that the value of segmentation metrics is validating the finding of visual analysis. In the Table 1, based on ground-truth SM-GT, it can be easily noted that, for segmentation output of the solar image captured on *Jan* obtained using FEDCM figure-out higher value (highlighted in bold and italic font) of dice coefficient and Jaccard index compared to the existing algorithms. In visual analysis of the particular result, it has been already found that output obtained using proposed technique is nearly similar to that of the ground-truth image of solar image taken on *Jan* compared to the other algorithms. Based on the data mentioned in the table it can be easily concluded that for the solar image captured on *Jan*, there is total increase of 14.66% in the value of dice coefficient and 22.5% increase in the value of Jaccard index achieved by FEDCM Algorithm compared to ACWE based technique. While for the same image, in Table 1, it highlights that SPoCA algorithm generate the better result. Since, the output obtained using SPoCA almost match the corresponding ground-truth RG-GT, which has also been used for calculating segmentation quality score in Table 1. However, the major concern associated with segmentation quality score estimation based on RG-GT is the selecting of initial seed points for region growing algorithm. If the seed points are not properly located, then this will lead to improper generation of ground-truth image for comparison purpose.

Similarly, the values of dice coefficient and Jaccard index obtained for the solar image *Sep* using FEDCM shown in Table 1, reflect the findings from the visual analysis. In this case, also, the introduced technique had shown its ability to extract the CHs regions far better than the existing algorithms. However, more interestingly it can be noted that in Table 1, CNN algorithm has show its promises in extracting CHs region accurately compared to other algorithm in few cases when compared with RG-GT. The main reason behind this is, the CNN model has been trained with the same RG-GT which has been used for calculation of quality score. Now, for the values of segmentation matrix shown from fourth, sixth, eleventh and fourteenth column of the Table 1, support the findings from the visual output figure-out in Figs. 4 and 5. As can be analysis from Section 4.4, in this case the coutour evolution using FEDCM has extract out several non-CHs region within CHs regions, compared to CHIMERA method of CHs detection, due to the ability of FEACM technique to tackle the topological changes and ambiguous object present in the image. As such, this presence of small pores in the final output reduce the segmentation score of the proposed algorithm.

Table 1
Coronal holes' segmentation quality score based on SM-GT and RG-GT, where above number represents dice coefficient and below represent the corresponding Jaccard index.

Methods	Ground-truth Used	Solar Image Captured on											
		Jan	Feb	Mar	Apr	May	Jun	Jul	Aug	Sep	Oct	Nov	Dec
ACWE Seg	SM-GT	0.7020	0.6550	0.5047	0.3895	0.6770	0.5658	0.6665	0.6100	0.7066	0.4603	0.6493	0.5636
		0.5408	0.4870	0.3375	0.2419	0.5117	0.3945	0.4998	0.4389	0.5463	0.2989	0.4807	0.3924
	RG-GT	0.8899	***0.8672***	0.7637	0.7237	0.7909	0.5655	0.5689	0.7363	0.7409	0.6542	0.6903	0.6141
		0.8017	***0.7655***	0.6178	0.5671	0.6541	0.3942	0.3975	0.5827	0.5885	0.4861	0.5271	0.4431
CNN Seg	SM-GT	0.6768	0.5901	0.4150	0.2929	0.6279	0.6786	0.6700	0.6009	0.7245	0.3693	0.6425	0.4947
		0.5114	0.4185	0.2618	0.1715	0.4577	0.5136	0.5038	0.4295	0.5680	0.2265	0.4733	0.3287
	RG-GT	0.7806	0.8400	0.6174	0.6782	0.7881	0.7140	***0.7543***	***0.8296***	0.8195	***0.7296***	0.6722	0.6184
		0.6401	0.7242	0.4465	0.5131	0.6503	0.5552	***0.6056***	***0.7088***	0.6943	***0.5743***	0.5063	0.4476
SPoCA	SM-GT	0.7070	0.6043	0.2550	0.3212	0.5648	0.3960	0.4675	0.5902	0.6752	0.3869	0.6473	0.5725
		0.5468	0.4329	0.1461	0.1913	0.3935	0.2469	0.3050	0.4186	0.5096	0.2399	0.4785	0.4011
	RG-GT	***0.8949***	0.8583	0.4484	0.5529	0.6811	0.3771	0.3660	0.7235	0.6916	0.4215	0.6527	0.5750
		0.8099	0.7518	0.2890	0.3821	0.5164	0.2323	0.2240	0.5668	0.5286	0.2670	0.4844	0.4035
CHIMERA	SM-GT	0.8010	***0.7377***	0.5195	***0.4509***	0.7820	0.7694	0.6483	0.6360	0.8625	***0.5386***	***0.8661***	***0.6932***
		0.6681	***0.5844***	0.3509	***0.2911***	0.6421	0.6253	0.4796	0.4663	0.7583	***0.3685***	***0.7638***	***0.5304***
	RG-GT	0.8473	0.8332	0.6788	0.7160	0.8188	0.7706	0.7004	0.7744	***0.8737***	0.6802	***0.8064***	***0.7948***
		0.7351	0.7141	0.5138	0.5576	0.6932	0.6268	0.5389	0.6319	***0.7757***	0.5154	***0.6756***	***0.6595***
FEDCM	SM-GT	***0.8247***	0.5905	***0.6029***	0.3810	***0.8137***	***0.7850***	***0.6873***	***0.6569***	***0.8671***	0.3719	0.7063	0.6470
		0.7017	0.4189	***0.4315***	0.2353	***0.6859***	***0.6460***	***0.5236***	***0.4891***	***0.7654***	0.2285	0.5460	0.4782
	RG-GT	0.8024	0.8133	***0.7760***	***0.8518***	***0.8616***	***0.8747***	0.5846	0.7304	0.8338	0.6524	0.6431	0.5309
		0.6701	0.6854	***0.6340***	***0.7419***	***0.7569***	***0.7773***	0.4131	0.5753	0.7150	0.4841	0.4740	0.3613

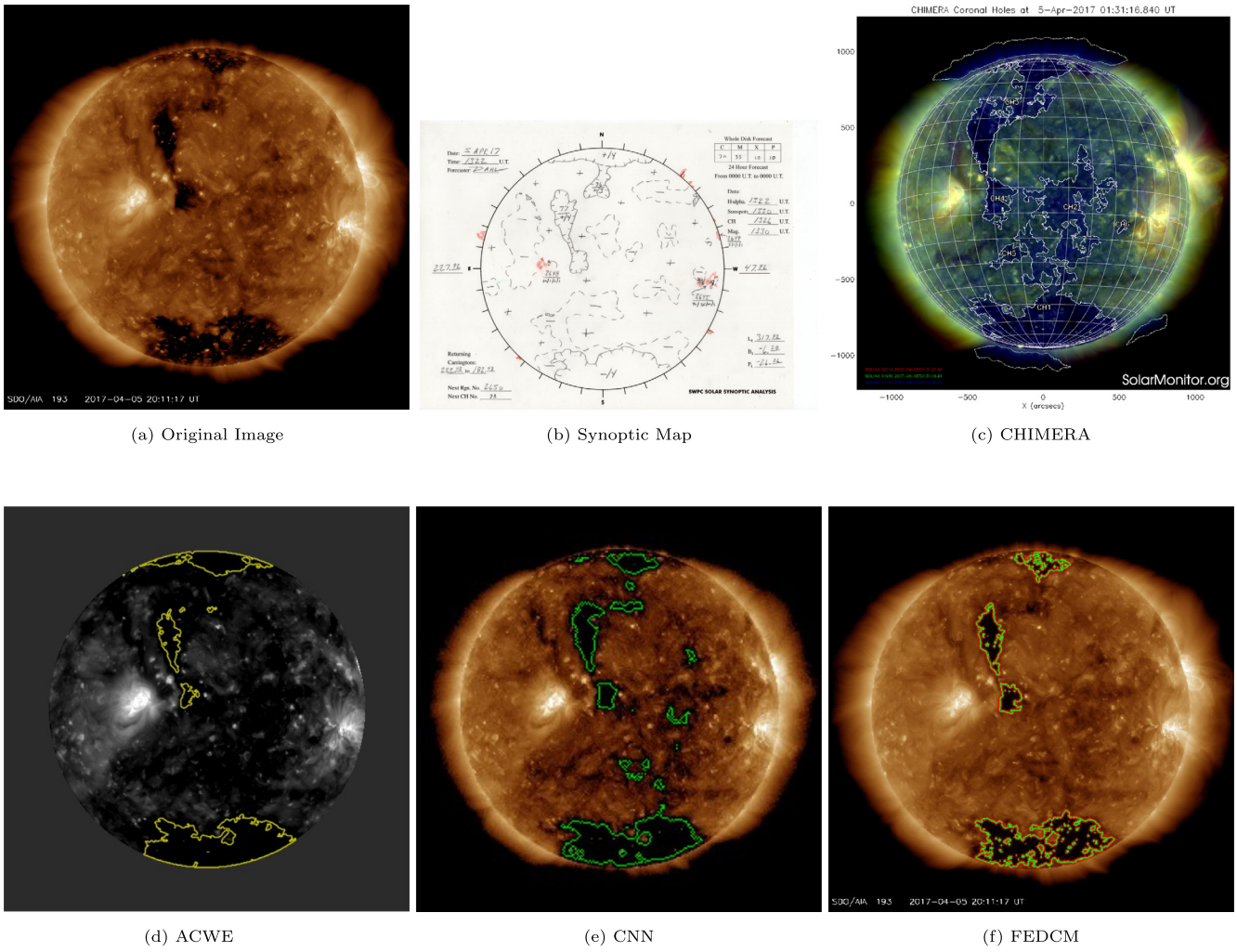

(a) Original Image (b) Synoptic Map (c) CHIMERA

(d) ACWE (e) CNN (f) FEDCM

Fig. 7. Comparison of results of CHIMERA with other existing methods for solar image captured on 2017-04-05.

Furthermore, while analyzing the output obtained using CHIMERA based on the segmentation quality score highlighted in Table 1, it can be concluded that the method able to detect CHs accurately in few cases, specially while comparing the output with respect to SM-GT image. However, if the visual analysis of CHIMERA based CHs segmentation results obtained from both; the code uploaded in github (results shown in Figs. 4 and 5), and the CHs segmentation catalog available in SolarMonitor[20](results shown in Figs. 7 and 8) is performed, a conclusion can be drawn easily that the method has over-segment the solar image in most of the cases. While analyzing Figs. 7 and 8, it has been found that CHIMERA has over-segment few region as CHs which has not been identified in synoptic map image. Similary, in Figs. 4f, 5b, 5d and 5f it can be easily seen that the method has over-segment the region. This is due to the fact that the method has a drawback in identifying vague CHs boundary arise due to occultation from brighter features (Garton et al., 2018). This over-segmentation will lead to estimation of CHs area with higher magnitude.

4.6. Time analysis

The performance of the implemented algorithm of FEDCM has also been evaluated in term of execution time taken to generate the results. The execution time of the compared models have been analysed by considering total time to reproduce the result for single solar image for the first time. All the compared algorithms of CHs detection have been executed on Intel(R) Core(TM) i5-8250U CPU with base frequency of 1.80 GHz and 4 GB RAM. For the completeness of the study, we also include the CNN algorithm time analysis, though not appropriate. While analyzing the execution time of CNN model for single image first time, total time required starting from training of the network to testing the network has been considered. This reflect the execution time of CNN model around 240 s. This execution time taken by CNN model is mainly due to train the network with large volume of dataset while reproducing the result for first time. However, it can be

[20] https://solarmonitor.org/.

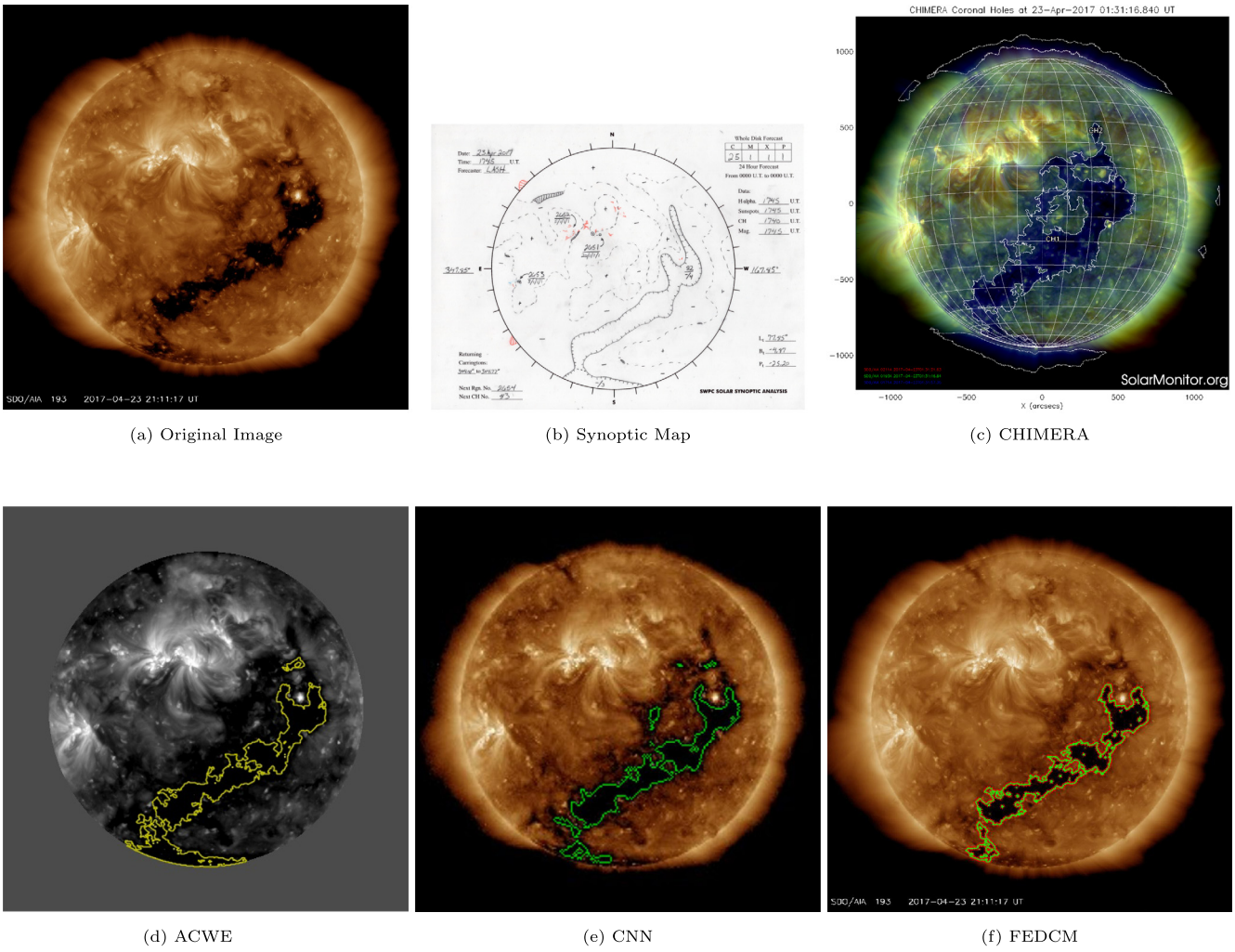

(a) Original Image (b) Synoptic Map (c) CHIMERA

(d) ACWE (e) CNN (f) FEDCM

Fig. 8. Comparison of results of CHIMERA with other existing methods for solar image captured on 2017-04-25.

noted that the performance of CNN models are optimized for GPU, which typically the speed up the performace 10–100 times faster compared to CPU. If single solar image is applied in a trained CNN model it will take considerably less time and single iteration to produce the result. It can also be noted that, despite of dealing with low resolution image CNN based technique is taking quite higher number of iterations (including training and testing) to perform the task of segmentation.

The execution time and the corresponding iteration taken by the algorithm to detect the CHs region in a single solar image has been displayed in Tables 2. From the table it can be noticed that, among the compared methods, ACWE is taking minimum iteration (highlighted in bold and italic font) to execute the segmentation task. Now, from the tables it can be seen that despite of taking higher number of iteration compared to ACWE method, and working with higher resolution image compared to both ACWE and CNN techniques, the proposed FEDCM takes quite less time (highlighted in bold and italic font) to execute the task of CHs segmentation. This is due to the fact that, FEDCM does not involve the gradient detection algorithm as exists in ACWE based technique, along side the proposed method does not require to train with large number of solar image sample to execute the results, like CNN based method. However, while compairing the execution time of FEDCM with SPoCA it can be found that FEDCM has comparable performance with that of the SPoCA. In most of the cases, it can be found that FEDCM stand second best in terms of computational time requirement. A summary of the comparative analysis has been drawn in Table 3.

4.7. Coronal holes area analysis

Performance of the compared methodologies has also been analysis in terms of percentage of CHs area extracted from the solar disk. The percentage of CHs area in solar disk estimated from the output image in terms of total percentage of pixels exists within the final contour detected using ACWE Seg, CNN Seg and FEDCM algorithms. While the percentage of CHs area in solar disk for

Table 2
Time and iteration for execution of coronal segmentation technique.

Images	Methods									
	ACWE Seg (on Image size 512 × 512)		CNN Seg (on Image size 256 × 256)		SPoCA (on Image size 4096 × 4096)		CHIMERA (on Image size 1024 × 1024)		Proposed Method (on Image size 1024 × 1024)	
	Time (sec)	Iteration	Time (sec)	Iteration	Time (sec)	Iteration	Time (sec)	Iteration	Time (sec)	Iteration
(a) Jan	141.7941	***3***	239.7257	357	***52.2209***	100	117.4300	25	58.2901	10
(b) Feb	140.5847	***3***	241.6426	357	***53.5869***	100	89.1225	25	60.6538	10
(c) Mar	141.6941	***3***	238.7274	357	***41.9048***	100	108.0168	25	59.3454	10
(d) Apr	139.8022	***3***	239.0552	357	***53.7006***	100	68.5132	25	62.3196	10
(e) May	140.1534	***3***	238.5822	357	***49.4854***	100	85.3057	25	55.0573	10
(f) Jun	139.7707	***3***	238.5443	357	***41.4631***	100	114.9441	25	56.7390	10
(g) Jul	141.8857	***3***	241.4772	357	***44.1775***	100	107.5324	25	59.3566	10
(h) Aug	139.2533	***3***	240.3188	357	***48.2032***	100	117.5695	25	55.4206	10
(i) Sep	141.7132	***3***	240.1994	357	***54.3626***	100	99.3444	25	54.8045	10
(j) Oct	141.6061	***3***	238.5798	357	54.4733	100	62.1427	25	***54.3214***	10
(k) Nov	139.0139	***3***	241.4121	357	***42.3642***	100	110.9478	25	58.3017	10
(l) Dec	140.1993	***3***	240.4882	357	54.5589	100	116.0396	25	***54.0659***	10

Table 3
Summary of comparitive analysis of the compared methods.

Methods	Type of Source File	Capturing Instrument	Wavelength	Image Resolution	Accuracy Analysis	Execution Time Analysis	Ranking based on Require Number of Iteration
ACWE Seg	level1 fits file	SDO/AIA	193 Å	512 × 512	It shows moderate performance while compared to FEDCM.	Takes moderately high computational time.	1
CNN Seg	jpeg image file	SDO/AIA	193 Å	256 × 256	It has second highest performance in terms of D_C while compared to FEDCM.	Reflect lowest performance in terms of execution time requirement for untrained network when computed in CPU.	5
SPoCA	level1 fits file	SDO/AIA	193 Å	4096 × 4096	It has least performance in terms of D_C when compared with SM-GT. However, when compared with RG-GT it shows satisfactory performance.	It takes quite less execution time compared to all other algorithm.	4
CHIMERA	level1.5 fits file	SDO/AIA SDO/HMI	171 Å, 193 Å, 211 Å, HMI Mag	1024 × 1024	It has comparable performance with FEDCM.	It take quite high execution time compared to SPoCA and FEDCM.	3
FEDCM	jpeg image file	SDO/AIA	193 Å	1024 × 1024	It reflect the highest D_C rate for most of the solar image while comparing with SM-GT. For case of comparision with RG-GT it gives out highest value of D_C for few cases.	It takes second least execution time and has comparable performance with that of SPoCA.	2

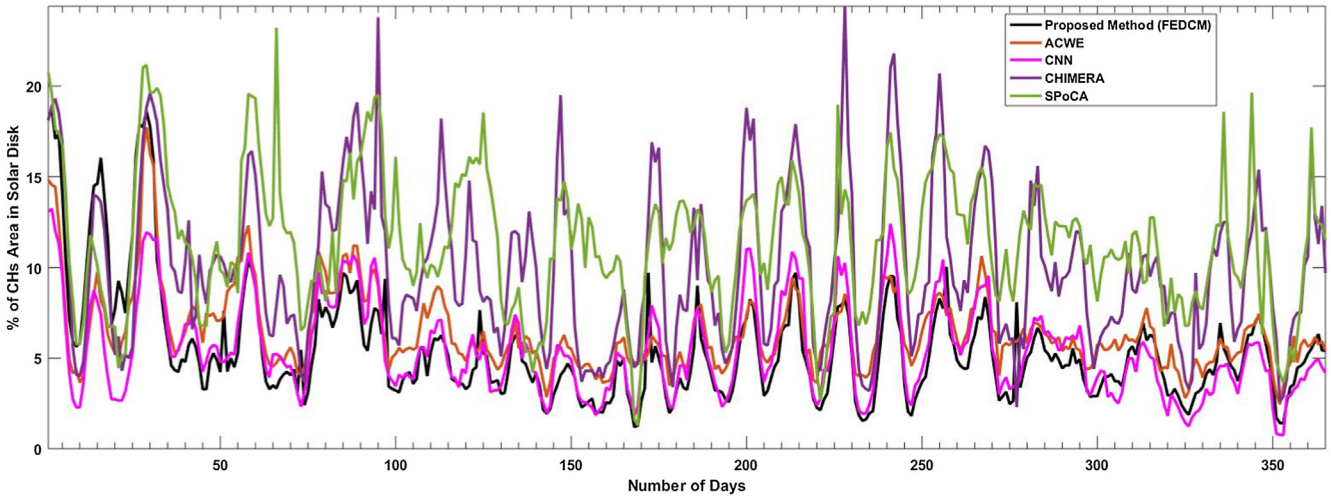

Fig. 9. CHs area detected for the year *2017*, using existing and proposed techniques.

CHIMERA and SPoCA has been collected from corresponding catalog available online. The percentage of CHs area in solar disk have been calculated for each day of the year 2017. Area of the CHs region has been estimated based on image morphological operation. Here, in the work hit-or-miss transformation has been use as a morphological operation with structuring element SE of radius 1. Mathematically, the operation implemented to an output image Bcan be expressed as:

$$B \circledast SE = (B \ominus SE_1) \bigcap (B^C \ominus SE_2), \tag{8}$$

where, SE_1 is set of elements of SE related to RoI and SE_2 set of elements of SE related to the background. The term B^C denotes complement of output image B. The term $(B \ominus SE_1)$ indicated output image morphological erosion operation with structuring element SE_1. Based on the obtained area of CHs $A_{coronal}$ the percentage of CHs area in solar disk is calculated as,

$$A_{CHs} = \frac{A_{coronal}}{\pi * R_p^2} \times 100; \tag{9}$$

where, R_p is the radius (in pixels) of the solar disk in image.

The percentage of CHs area observed has been plotted in the graph shown in Fig. 9. The graph reflects the percentage of area analyzed by FEDCM is consistent with the percentage of CHs area analyzed by ACWE and CNN algorithm, for any particular day of the year. From graph it can be seen that CHIMERA[21] and SPoCA[22] gives higher magnitude for the percentage of area as obtained from the catalog. This may be due to the fact that the methods sometimes oversegment the solar disk region (specially in case of CHIMERA (Garton et al., 2018)). Another reason may be due to the change in area calculation method in SPoCA and CHIMERA. It is to be, however, noted that the trend of both SPoCA as-well-as CHIMERA matches very well with the proposed method.

5. Conclusions

In this work a circular Hough transformed inspired fuzzy energy-based dual contours method (FEDCM) of segmentation has been proposed for the detection and extraction of CHs regions from the solar disk image. Here, in this work two contours has been initialized simultaneously on the solar disk boundary in the solar image using circular hough transform algorithm for the purpose of segmentation using FEDCM. In the work, one contour has been initialize for executing the task of solar image segmentation using FEACM, while other contour has been initialize to extract out the CHs region from the segmented image. The method has been applied on SDO/AIA solar images of 193 Å wavelength for a single year. From the experiment conducted, it has been found that the proposed method is capable of generating the desire results within less execution time without affecting the original resolution of the SDO/AIA solar image used in the experiment. The proposed algorithm has three major advantages. These are, firstly, the algorithm has capability to extract proper CHs region in-spite of the presence of vague boundaries at the CHs regions unlike other existing algorithms, due to incorporation of fuzzy technique. Secondly, due to the application of circular Hough transformation, the contour initialization problem as present in the work (Boucheron et al., 2016) has been overcome, moreover, it does not require exact data of solar disk center co-ordinate and solar disk radius for initialization of the contour for proposed algorithm and for limb correction, like other existing algorithms. Thirdly, it does not require training with large database of solar image for proper generation of output, unlike neural network based method of CHs detection (Illarionov

[21] https://solarmonitor.org/data.
[22] https://www.lmsal.com/hek/isolsearch/isolsearch.html.

and Tlatov, 2018). However, for few SDO/AIA solar image it has been found that the performance of the proposed technique is not satisfactory which may cause be due to the contour get stuck at the local minima or due improper selection of parameters for that particular image. Thus it will be in future focus to develop an algorithm in order to overcome the effect of local minima. Side-by-side, it will also be in focus to develop an automated technique in order to select proper parameters for the fitting function. Testing of the proposed algorithm on solar images with wavelength value other than 193 Å is also to be carried out in upcoming works.

Acknowledgement

The financial support received under DST INSPIRE Faculty grant is thankfully acknowledged. We would also like to acknowledge Dr. Laura Boucheron and Dr. Egor Illarionov for their constant assistance in our work.

Appendix A. Circular Hough transform

The implementation of the circular Hough transform had been done with an assumption that if a circle in a image is parameterized by its radius r and center (a,b), then it is connected with co-ordinates of edge points (x,y), for which the circle equation is given by;

$$r^2 = (x-a)^2 + (y-b)^2, \tag{A.1}$$

which indicates, that any given edge points (x_i, y_i) could lie on points of any circle whose parameters reside on the surface of right circular cone in (a,b,r) dimensional space. If the cones comparing to numerous edge focuses cross at a single point, at that point all the picture focuses lie on the circle characterized by those three parameters, as highlighted in Fig. A.10 (Yuen et al., 1990). The detected circle with radius $r$and center (a,b) is considered as the initial circular contour for the FEACM and FSC. The steps involved in detection of circle using Hough transform has been illustrated in Algorithm 1.

Algorithm 1. Circular Hough Transform

1: **Input:** Image I
2: **Initialization**: Accumulator array $A[a,b,r] = 0$
3: Filter image using Gaussian convolution
4: Convert image into gray-scale
5: Apply Canny operator to detect edge
6: **for** Each edge pixel (x,y) **do**
7: **for** Radius $r = r_{min} : r_{max}$ **do**
8: **for** $\theta = 0 : 360$ **do**
9: $a = x - r * \ cos(\theta * \ \pi/180)$
10: $b = y - r * \ sin(\theta * \ \pi/180)$
11: $A[a,b,r] = A[a,b,r] + 1$
12: Possible vale of $[a,b,r]$ is given by maxima in array A
13: **Output:** Detect circle in the image given by $r^2 = (x-a)^2 + (y-b)^2$.

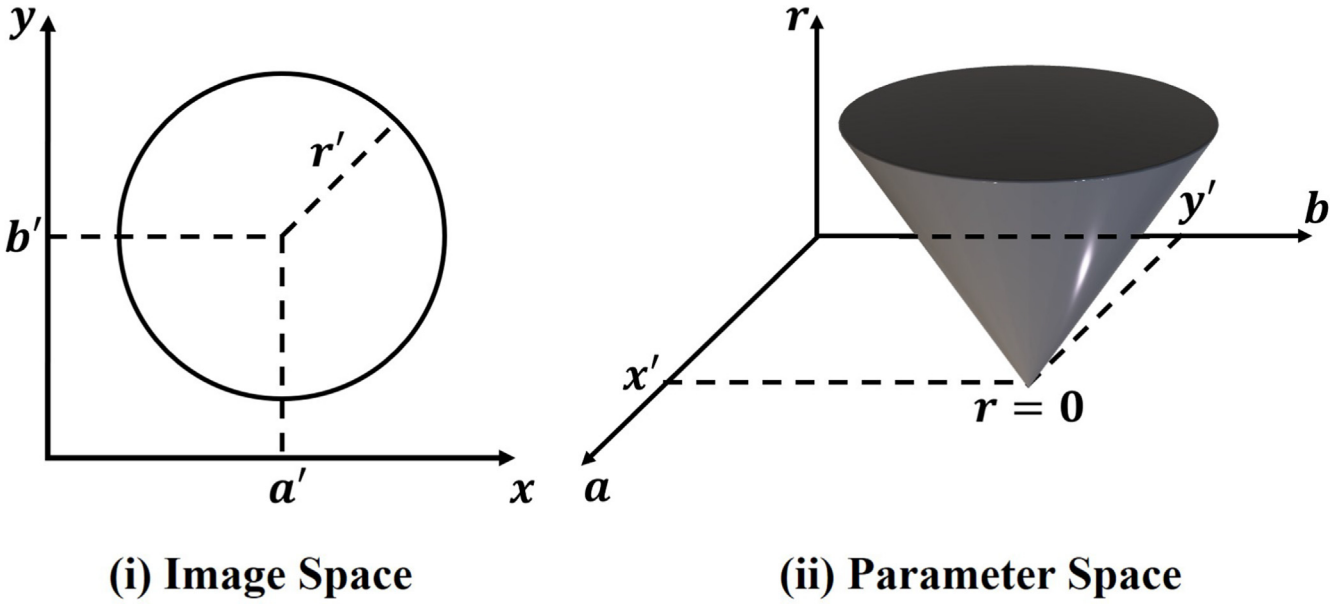

Fig. A.10. Diagrammatic representation of circular Hough transform.

Algorithm 2. FEDCM based CHs Segmentation

1: **Input:** Image I
2: **Initialization**: $\mu = 0, \lambda_1, \lambda_2 > 0$ and other parameters
3: Initialize two circular contours ϕ_1 and ϕ_2 using Algorithm 1
4: Set $u_o > 0.5$ for pixels in I^i and $u_o < 0.5$ for pixels in I^o
5: **for** iter = 1:max_iter **do**
6: Compute c_1 and c_2 using Eqs. (B.1) and (B.2) respectively
7: Calculate u_n using Eq. (B.3)
8: Calculate $\triangle F$ using Eq. (B.4)
9: **if** $\triangle F < 0$ **then**
10: $u_o \longleftarrow u_n$
11: **else**
12: $u_o \longleftarrow u_o$
13: **goto** Step 7; Compute the total energy F of the image using Jacobi iterations
14: **if** Total energy Fremains unchanged **then**
15: **goto** Step 6
16: **else**
17: **goto** Step 20
18: **break**;
19: Set contour C_0 as final contour
20: Set pixels in I^i as foreground and in I^o as background
21: **if** $u(x,y)_n < 0.5$ and $u(x,y)_S > 0.5$ **then**
22: Label *pixel*$\longleftarrow$*foreground*
23: **else if** $u(x,y)_n > 0.5$ and $u(x,y)_S < 0.5$ **then**
24: Label *pixel*$\longleftarrow$*background*
25: **else** $u(x,y)_n > 0.5$ and $u(x,y)_S > 0.5$
26: Label *pixel*$\longleftarrow$*background*
27: **Output:** *foreground* pixels are CHs pixels for image I.

Appendix B. Numerical approximation

In Eqs. (3) and (5), c_1 and c_2 denotes the average prototypes of region inside and outside the curve Crespectively, which is denoted by equations;

$$c_1 = \frac{\int_\Omega [u(x,y)]^m I(x,y)dxdy}{\int_\Omega [u(x,y)]^m dxdy}, \tag{B.1}$$

and

$$c_2 = \frac{\int_\Omega [1-u(x,y)]^m I(x,y)dxdy}{\int_\Omega [1-u(x,y)]^m dxdy}. \tag{B.2}$$

Here, in stated equations degree of membership for $I(x,y)$ is represented by $u(x,y)$, which is given by equation;

$$u(x,y) = \frac{1}{1+\left(\frac{\lambda_1 (I(x,y)-c_1)^2}{\lambda_2 (I(x,y)-c_2)^2}\right)^{\frac{1}{m-1}}}. \tag{B.3}$$

Now, corresponding membership value for pixel $P$with intensity value I_o is denoted by u_o, which change to u_n based on Eq. (B.3). Therefore energy difference due to change of membership value can be given as;

$$\triangle F = \lambda_1 s_1 \frac{[u_n^m - u_o^m](I_o - c_1)^2}{s_1 + u_n^m - u_o^m} + \lambda_2 s_2 \times \frac{[(1-u_n)^m - (1-u_o)^m](I_o - c_2)^2}{s_2 + (1-u_n)^m - (1-u_o)^m}, \tag{B.4}$$

where, the term s_1 denotes sum of weighted membership, which is represented by $s_1 = \sum_\Omega [u(x,y)]^m$. Where as, the term s_2 is represented by $s_2 = \sum_\Omega [1-u(x,y)]^m$.

Appendix C. Proposed FEDCM algorithm

The algorithm of the introduced CHs segmentation has been given in Algorithm 2.

Appendix D. Block-diagram of the proposed FEDCM

The block-diagram of the proposed FEDCM based CHs detection in SDO/AIA solar image has been shown in Fig. D.11.

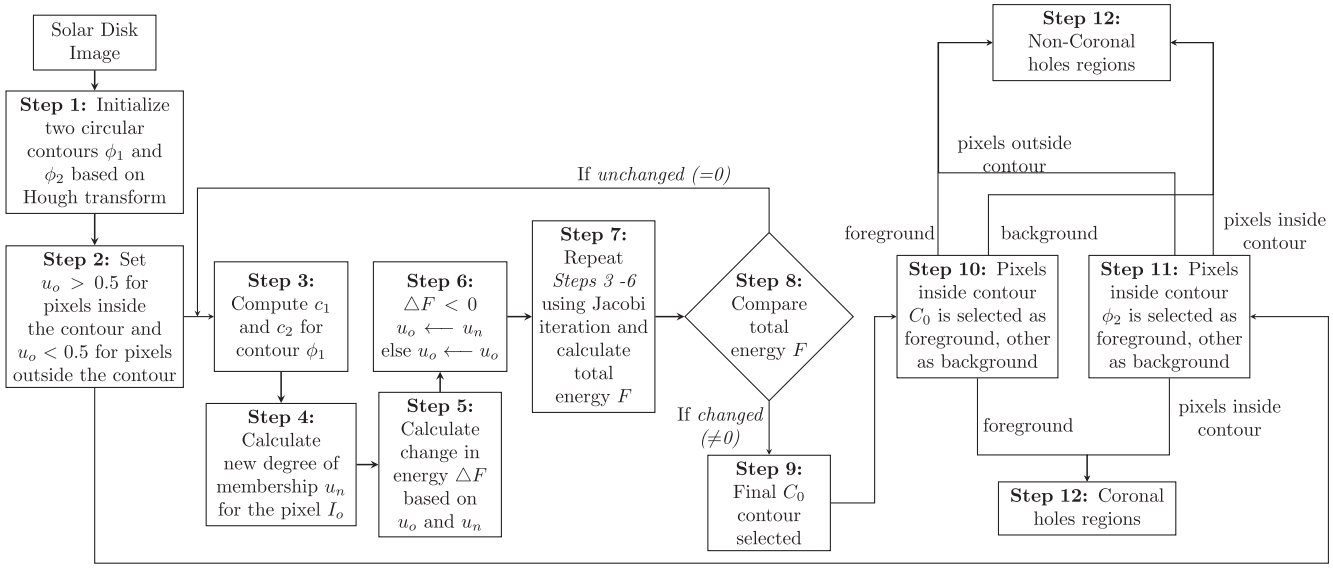

Fig. D.11. Block-diagram of the proposed work.

Appendix E. Discussion about the contour evolution

Contours evolution is a vital steps in FEDCM based CHs segmentation. The initial contours setup for FEDCM has been shown in second row of Figs. E.12 and E.13. Here in the work, two circular contours have been setup on the boundary of the solar disk as shown in the Figs. E.12 and E.13. After the execution of FEACM, it has been found that

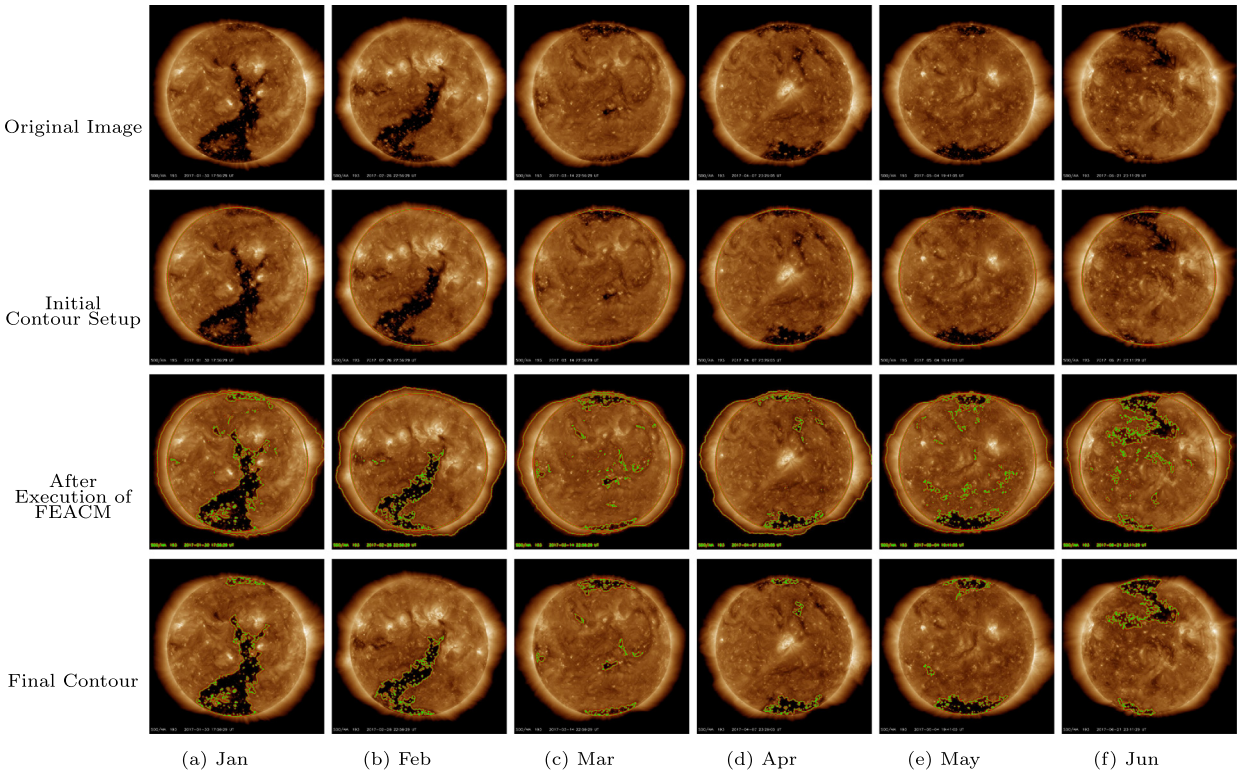

Fig. E.12. Contour evolution at various stages of FEDCM tested on solar images for the period of Jan-Jun.

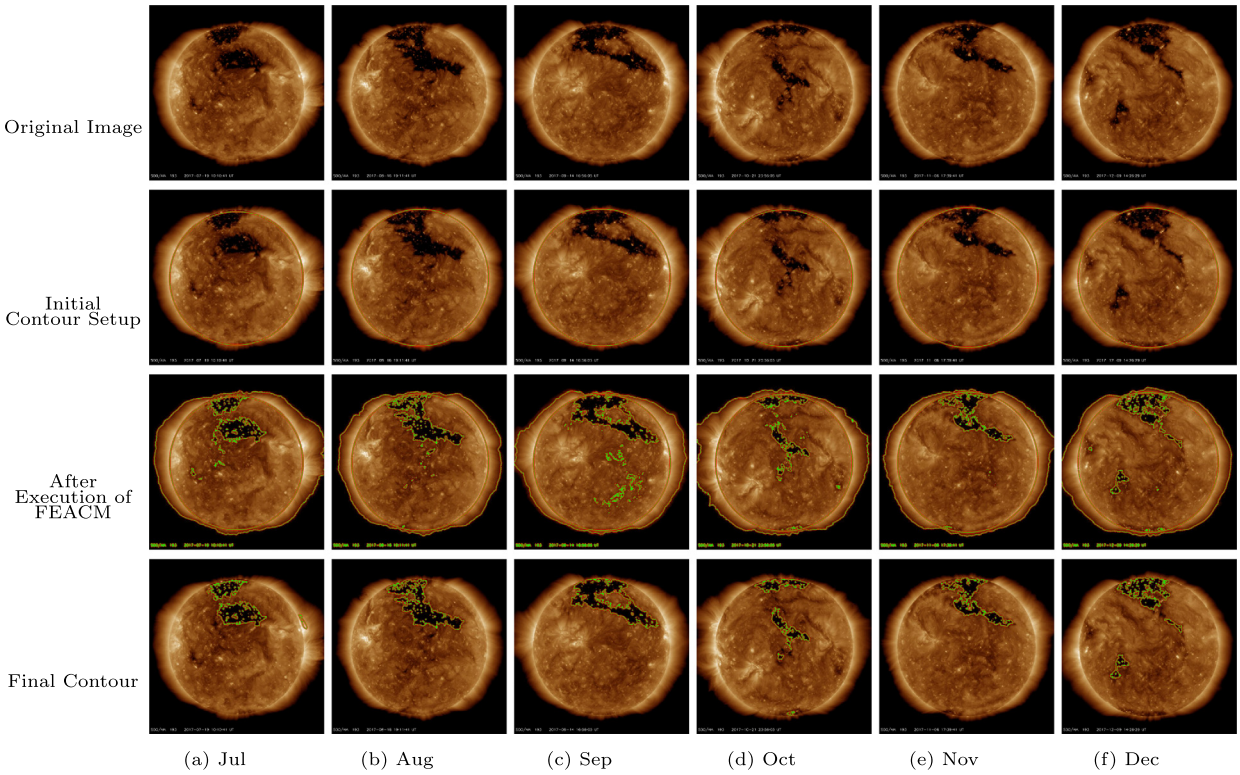

Fig. E.13. Contour evolution at various stages of FEDCM tested on solar images for the period of Jul-Dec.

one contour segment the SDO/AIA solar image foreground and background, while the other contour still remain static on the boundary of the solar disk in the image. The corresponding curve deformation have been displayed in the third row of E.12 and E.13. From the same rows it can be noticed that FEACM has circumscribe many small unwanted region apart from CHs, solar disk region, and solar limbs. In order to tackle this redundant region, a postprocessing (as described in Meng et al. (2013)) has been done after the accomplishment of FEACM. In this method, in the first stage all the disjoined region are identified. In the next stage, the areas of all the disjoined regions $(D_0, D_1, \ldots, D_a)$ are estimated, such that $D = D_0, D_1, \ldots, D_a, a \in \mathbb{Z}$, where a is the total number of disjoined regions. Now in order to remove the redundant regions, the disjoined regions with $D_n > T$ has been considered as the RoI, where T is a threshold. In the experiment, $T = 0.05 \max(D)$ has been set for all the output image obtained after accomplishment of FEACM. The final contour position obtained after the postprocessing steps and implementation FSC has been shown in the last row of the Figs. E.12 and E.13.

References

Bandyopadhyay, S., 2018. Object of interest detection in video sequence using co-segmentation: a new era in video surveillance. In: 2018 4th International Conference on Recent Advances in Information Technology (RAIT), pp. 1–6.

Barra, V., Delouille, V., Kretzschmar, M., Hochedez, J.-F., 2009. Fast and robust segmentation of solar euv images: algorithm and results for solar cycle 23. Astron. Astrophys. 505 (1), 361–371.

Bora, D.J., Gupta, D., Kumar, A., 2014. A comparative study between fuzzy clustering algorithm and hard clustering algorithm. arXiv preprint arXiv:1404.6059.

Boucheron, L.E., Valluri, M., McAteer, R.T.J., 2016. Segmentation of coronal holes using active contours without edges. Sol. Phys. 291 (8), 2353–2372. https://doi.org/10.1007/s11207-016-0985-z.

Bresenham, J.E., 1965. Algorithm for computer control of a digital plotter. IBM Syst. J. 4 (1), 25–30.

Caselles, V., Kimmel, R., Sapiro, G., 1997. Geodesic active contours. Int. J. Comput. Vision 22 (1), 61–79. https://doi.org/10.1023/A:1007979827043.

Chan, T.F., Vese, L.A., 2001. Active contours without edges. IEEE Trans. Image Process. 10 (2), 266–277.

Ciecholewski, M., 2015. Automated coronal hole segmentation from solar euv images using the watershed transform. J. Vis. Commun. Image Represent. 33, 203–218 http://www.sciencedirect.com/science/article/pii/S1047320315001856.

Darolti, C., Mertins, A., Bodensteiner, C., Hofmann, U.G., 2008. Local region descriptors for active contours evolution. IEEE Trans. Image Process. 17 (12), 2275–2288.

Delouille, V., Hofmeister, S.J., Reiss, M.A., Mampaey, B., Temmer, M., Veronig, A., 2018. Coronal holes detection using supervised classification. In: Camporeale, E., Wing, S., Johnson, J.R. (Eds.), Machine Learning Techniques for Space Weather. Elsevier, pp. 365–395, http://www.sciencedirect.com/science/article/pii/B9780128117880000159.

Duda, R.O., Hart, P.E., Jan. 1972. Use of the hough transformation to detect lines and curves in pictures. Commun. ACM 15 (1), 11–15. https://doi.org/10.1145/361237.361242.

Fang, J., Liu, H., Zhang, L., Liu, J., Liu, H., 2019. Fuzzy region-based active contours driven by weighting global and local fitting energy. IEEE Access, 1.

Garton, Tadhg M., Gallagher, Peter T., Murray, Sophie A., 2018. Automated coronal hole identification via multi-thermal intensity segmentation. J. Space Weather Space Clim. 8, A02. https://doi.org/10.1051/swsc/2017039.

Gosling, J., Pizzo, V., 1999. Formation and evolution of corotating interaction regions and their three dimensional structure. Space Sci. Rev. 89 (1), 21–52. https://doi.org/10.1023/A: 1005291711900.

Gunn, S.R., Nixon, M.S., 1997. A robust snake implementation; a dual active contour. IEEE Trans. Pattern Anal. Mach. Intell. 19 (1), 63–68.

Harvey, K.L., Recely, F., 2002. Polar coronal holes during cycles 22 and 23. Sol. Phys. 211 (1), 31–52. https://doi.org/10.1023/A:1022469023581.

Hough, P.V., 1962. Method and means for recognizing complex patterns. US Patent 3,069,654.

Huang, C., Zeng, L., 2015. An active contour model for the segmentation of images with intensity inhomogeneities and bias field estimation. PloS one 10 (4), e0120399.

Illarionov, E.A., Tlatov, A.G., 2018. Segmentation of coronal holes in solar disc images with a convolutional neural network. Mon. Not. R. Astron. Soc. 481 (4), 5014–5021.

Kirk, M.S., Pesnell, W.D., Young, C.A., Hess Webber, S.A., 2009. Automated detection of euv polar coronal holes during solar cycle 23. Sol. Phys. 257 (1), 99–112. https://doi.org/10.1007/s11207-009-9369-y.

Krieger, A.S., Timothy, A.F., Roelof, E.C., 1973. A coronal hole and its identification as the source of a high velocity solar wind stream. Sol. Phys. 29 (2), 505–525. https://doi.org/10.1007/BF00150828.

Krinidis, S., Chatzis, V., 2009. Fuzzy energy-based active contours. IEEE Trans. Image Process. 18 (12), 2747–2755.

Krista, L.D., Gallagher, P.T., 2009. Automated coronal hole detection using local intensity thresholding techniques. Sol. Phys. 256 (1), 87–100. https://doi.org/10.1007/s11207-009-9357-2.

Kucuk, A., Banda, J.M., Angryk, R.A., 2017. A large-scale solar dynamics observatory image dataset for computer vision applications. Sci. data 4, 170096.

Lemen, J.R., Title, A.M., Akin, D.J., Boerner, P.F., Chou, C., Drake, J. F., Duncan, D.W., Edwards, C.G., Friedlaender, F.M., Heyman, G. F., Hurlburt, N.E., Katz, N.L., Kushner, G.D., Levay, M., Lindgren, R.W., Mathur, D.P., McFeaters, E.L., Mitchell, S., Rehse, R.A., Schrijver, C.J., Springer, L.A., Stern, R.A., Tarbell, T.D., Wuelser, J.-P., Wolfson, C.J., Yanari, C., Bookbinder, J.A., Cheimets, P.N., Caldwell, D., Deluca, E.E., Gates, R., Golub, L., Park, S., Podgorski, W.A., Bush, R.I., Scherrer, P.H., Gummin, M.A., Smith, P., Auker, G., Jerram, P., Pool, P., Soufli, R., Windt, D.L., Beardsley, S., Clapp, M., Lang, J., Waltham, N., 2012. The atmospheric imaging assembly (aia) on the solar dynamics observatory (sdo). Sol. Phys. 275 (1), 17–40. https://doi.org/10.1007/s11207-011-9776-8.

Luxburg, U.V., Bousquet, O., 2004. Distance-based classification with lipschitz functions. J. Mach. Learn. Res. 5 (Jun), 669–695.

Meng, F., Li, H., Liu, G., Ngan, K.N., 2013. Image cosegmentation by incorporating color reward strategy and active contour model. IEEE Trans. Cybernet. 43 (2), 725–737.

Munro, R.H., Withbroe, G.L., 1972. Properties of a coronal "hole" derived from extreme-ultraviolet observations. Astrophys. J. 176, 511.

Nieniewski, M., 2004. Extraction of diffuse objects from images by means of watershed and region merging: example of solar images. IEEE Trans. Syst. Man Cybernet. Part B (Cybernet.) 34 (1), 796–801.

Osher, S., Sethian, J.A., 1988. Fronts propagating with curvature-dependent speed: algorithms based on hamilton-jacobi formulations. J. Comput. Phys. 79 (1), 12–49 http://www.sciencedirect.com/science/article/pii/0021999188900022.

Poria, S., Poria, S., Dhiman, A., Dhiman, A., 2017. Existence and uniqueness of solution to odes: Lipschitz continuity. Resonance 22 (05).

Reiss, Martin A., Hofmeister, Stefan J., Visscher, De, Ruben, Temmer, Manuela, Veronig, Astrid, M., Delouille, Véronique, Mampaey, Benjamin, Ahammer, Helmut, 2015. Improvements on coronal hole

detection in sdo/aia images using supervised classification. J. Space Weather Space Clim. 5, A23. https://doi.org/10.1051/swsc/2015025.

Rotter, T., Veronig, A.M., Temmer, M., Vršnak, B., 2012. Relation between coronal hole areas on the sun and the solar wind parameters at 1 au. Sol. Phys. 281 (2), 793–813. https://doi.org/10.1007/s11207-012-0101-y.

Scholl, I.F., Habbal, S.R., 2009. Automatic Detection and Classification of Coronal Holes and Filaments Based on EUV and Magnetogram Observations of the Solar Disk. Springer, New York, doi: 10.1007/978-0-387-98154-3_16.

Verbeeck, C., Delouille, V., Mampaey, B., De Visscher, R., 2014. The spoca-suite: Software for extraction, characterization, and tracking of active regions and coronal holes on euv images. Astron. Astrophys. 561, A29.

Wang, L., Chang, Y., Wang, H., Wu, Z., Pu, J., Yang, X., 2017. An active contour model based on local fitted images for image segmentation. Inf. Sci. 418–419, 61–73 http://www.sciencedirect.com/science/article/pii/S0020025516308556.

Wang, Y., He, C., 2012. Adaptive level set evolution starting with a constant function. Appl. Math. Model. 36 (7), 3217–3228 http://www.sciencedirect.com/science/article/pii/S0307904X11006779.

Xie, X., Mirmehdi, M., 2010. Initialisation-free active contour segmentation. In: 2010 20th International Conference on Pattern Recognition, pp. 2318–2321.

Xingfei, G., Tian, J., 01 2002. An automatic active contour model for multiple objects. vol. 2. pp. 881–884.

Yuen, H., Princen, J., Illingworth, J., Kittler, J., 1990. Comparative study of hough transform methods for circle finding. Image Vision Comput. 8 (1), 71–77.